Chevychelov V.Y., Viryus A.A. Study of F and Cl partition between biotite crystallizing from melt and granite melt at subliquidus conditions. *UDC 550.42*

Korzhinskii Institute of Experimental Mineralogy RAS; Moscow district chev@iem.ac.ru, allavirus@yandex.ru

Abstract. The compositions of micas (biotites) are very sensitive to changes in the physico-chemical conditions of mineral formation (acidity-alkalinity, fluid saturation, T, f_{O2}, etc.), so experimental data on phase equilibria in silicate systems involving micas and volatile components are of particular interest for understanding the conditions of formation of igneous rocks and related ores. We have studied in detail the chemical compositions of natural biotites of the Khangilai massif (Eastern Transbaikalia), including the F and Cl contents. Then, experiments were carried out on the crystallization of biotite from the melt of the Khangilai granites at subliquidus conditions (T = 690 - 760°C and P ~ 100 - 500 MPa).

As a result of the studies, it was established that during crystallization of the Khangilai granite massif, the F/Cl ratios in the melt could vary in a wide range from 1 to 12 or more. F/Cl ratios in the biotites of this massif were significantly higher ~ 22 - 34, which is due to the high affinity of F to biotite, and Cl to the melt. The average contents of F and Cl in biotite were approximately 1.4 wt.% and 0.05 wt.%, respectively. The main results, illustrated by diagrams of the obtained dependencies, are considered in more detail in another report by V.Yu. Chevychelov and A.A. Viryus "The effect of pressure and melt composition on the partition of F and Cl in the biotite - granite melt system".

***Keywords**: physical and chemical conditions of formation; compositions of micas; temperature; pressure; crystallization of granite melt; experiment*

Introduction. The compositions of micas (biotites) are very sensitive to changes in the physico-chemical conditions of mineralization (acidity-alkalinity, fluid saturation, T, f_{O2}, etc.), so experimental data on phase equilibria in silicate systems involving micas and volatile components are of particular interest for understanding the conditions of formation of igneous rocks and related ores. The topic of research was chosen due to the need to clarify the physico-chemical parameters of formation of biotite granites of the Khangilai massif (Eastern Transbaikalia), with magmatic differentiates of which the Orlovskoye tantalum and Spokoininskoye tungsten deposits are associated (Zaraisky et al., 2008). The conditions of genesis of the Khangilai massif granites were as follows. According to geological data, the roof of the massif was located at a depth of about 2-3 km from the paleosurface, which corresponds to a lithostatic pressure of 50-80 MPa. In the lower parts of the massifs with a vertical thickness of up to 8 km, the pressure could reach 200-300 MPa, and during retrograde boiling of magma it could briefly increase even higher. Partially, this high pressure could be transmitted to the upper horizons, which obviously explains the pressure values of 300-500 MPa, established by the results of studying fluid inclusions. The crystallization temperature of the Khangilai massif could be from 700 to 800°C. The water concentration in the melt was 2.5-4.8 wt.% (the melt was close to water saturation), and the F concentration was below 1 wt.% (oral communication by Kotelnikova Z.A.; Reyf et al., 2000; Reyf, 1990).

Research methods. Using different geothermometers (Zr in rutile and Ti in zircon; Zr/Hf in zircon; Ti in quartz), the crystallization temperature of the Khangilai massif granites was estimated. The chemical compositions of natural biotites of the Khangilai massif, including the F and Cl contents, were studied in detail. For further experimental studies, primary melting of a sample of the Khangilai massif granites was carried out (Table 1). Then, biotite crystals were grown from the obtained melt with the addition of F- and Cl-containing fluids at subliquidus conditions, and after the experiments, the chemical compositions of the biotite crystals and granite melt were determined. In order to estimate the effect of pressure on the composition of crystallizing biotites, the experiments were carried out at pressures of 110, 315, 450 and 535 MPa. The following aqueous solutions were used in the experiments: 5M HF + 5M HCl; 1M HF + 1M HCl; 2M HF + 2M KF; 5M HF + 1M HCl; 0.33M HCl + 0.33M NaCl + 0.33M KCl and H_2O.

Table 1. Chemical composition of granite glass obtained by melting granites of the Khangilai massif (T = 1350°C, P = 0.1 MPa, unwelded shut capsule, duration 1 day; analyses according to EDS data, F and Cl according to wave spectrometer data, in wt. %, normalized to 100 %)

Experience number	SiO_2	TiO_2	Al_2O_3	FeO_{tot}	MnO	MgO	CaO	Na_2O	K_2O	F	Cl	Total
VZ-1/melt	75.69	0.23	13.67	1.27	0.05	0.36	0.82	3.73	4.04	0.12	0.01	100.00

Fig. 1. Internally heated pressure vessel (IHPV).

The experiments were prepared and conducted as follows. First, a finely crushed sample of the initial granite, placed in an unwelded shut large platinum capsule (9 mm × 0.2 mm × 50 mm), was melted under alundum gate in KO-14 furnace at T = 1350°C, P = 0.1 MPa and duration of 1 day. (Table 1). The resulting granite glass, ground into powder, was placed in small platinum capsules (4 mm × 0.2 mm × 20 mm), with F- and Cl-containing solutions poured into the bottom. Then the capsule was welded shut. The initial weight ratio of solution/granite glass was from 1 to 5 to 1 to 10, depending on the pressure in the experiment. The experiments on crystallization of granite glass were conducted in internally heated pressure vessels (IHPV, Fig. 1) pressurized with pure Ar gas. The following T regime was used: first, at T = 830 (800)°C and the required pressure, the capsules were kept for 1 day for complete melting of the glass in water-saturated conditions, and then the temperature was lowered to 720 (690, 760)°C and the experiments continued for another 9 to 13 days for crystallization of minerals in the melt.

After the experiments, the chemical compositions of the synthesized phases and minerals, as well as the concentrations of F and Cl in biotite and in the quenched granite glass, were determined by X-ray spectral microanalysis (XSMA) on a Tescan Vega II XMU scanning electron microscope (SEM) using energy-dispersive (EDS, INCAx-sight) and wave (WDS, INCA Wave 700) X-ray spectrometers.

Main results. According to the results of petrographic study of the sample of medium-grained biotite granites of the Khangilai massif, two types of biotites (biotite 1 and biotite 2) were determined in thin section, differing in chemical composition (Table 2). Biotite 1 is one of the first minerals to crystallized from granite melt. Its crystals have smooth edges, which are in good agreement with the boundaries of the main rock-forming minerals: quartz, K-feldspar and plagioclase. The fluorine and chlorine contents in these biotites were determined with high accuracy using a precision wave spectrometer. The obtained results were compared with the analyses of micas (biotites) synthesized in the experiments.

The products obtained as result of the experiments consisted of granite glass (Table 3) and very small amount of crystalline phases (less than 1 vol. %), represented mainly by mica (biotite) and accessory minerals (apatite, zircon, monazite). The crystal sizes usually did not exceed 10-20 μm. Flat biotite crystals in cross-section looked like elongated plates up to 4-5 μm thick (Fig. 2).

Table 2. Chemical composition of natural biotites from the Khangilai granite massif (according to EDS data, F and Cl according to wave spectrometer data, in wt. %, normalized to 100%)

	SiO_2	TiO_2	Al_2O_3	FeO_{tot}	MnO	MgO	K_2O	F[1]	Cl[1]	Total	F/Cl[1]	$Mg^{\#}$ [2]
Biotite 1	38.05	3.38	17.40	24.17	0.33	5.57	9.66	1.07-1.77/ 1.39	0.02-0.07/ 0.05	100.00	22.2-34.2/ 27.4	43.76
Biotite 2	49.71	0.66	30.08	5.02	0.10	2.30	11.05	0.77-1.37/ 1.07	0-0.020/ 0.004	100.00	62.3-1117/ 274.3	55.04

[1] Content range and average content. [2] $Mg^{\#}$ - magnesia coefficient equal to the mole ratio 100×Mg/ (Mg+Mn+Fe).

Table 3. Chemical composition of granite glasses obtained in experiments VZ-5/sol and VZ-6/sol (according to EDS data, F and Cl according to wave spectrometer data, in wt. %, normalized to 100 %)

Solution	Experience number	P, MPa/ T, °C	SiO_2	Al_2O_3	FeO_{tot}	MgO	CaO	Na_2O	K_2O	F	Cl	Total	F/Cl
Sol-2 – 1M HF + 1M HCl	VZ-5/sol	110/ 720	76.57	13.80	0.59	0.18	0.89	3.20	4.28	0.25	0.23	100.00	1.10
	VZ-6/sol	315/ 690	77.38	13.51	0.33	0.37	0.78	2.86	4.29	0.35	0.12	100.00	3.08

Solution	Experience number	*P*, MPa/ *T*, °C	SiO_2	Al_2O_3	FeO_{tot}	MgO	CaO	Na_2O	K_2O	F	Cl	Total	F/Cl
Sol-4 – 5M HF + 1M HCl	VZ-5/sol	110/ 720	76.22	13.65	0.60	0.17	0.81	3.13	4.20	0.99	0.23	100.00	4.37
	VZ-6/sol	315/ 690	77.00	13.23	0.26	0.32	0.84	2.64	4.26	1.33	0.12	100.00	11.60

The chemical composition of the micas obtained in the experiments (Table 4), according to the XSMA data, is compared with the composition of biotite from natural Khangilai granites and is close to the composition of biotite from the reference book (Rieder et al., 1999). Analyses of natural biotites had sums of 94–97 wt. %, and sums in the analyses of synthesized biotites usually ranged from 97 to 102 wt. %. High sums in biotite analyses may indicate a low content of H_2O and the OH^- group in their composition. The magnesia coefficient ($Mg^{\#}$ = mole ratio 100×Mg/ (Mg+Mn+Fe)) of the synthesized micas varies in the range from 63 to 85 and is significantly higher than the $Mg^{\#}$ coefficient of natural biotites of the Khangilai massif (from 40 to 57). The increased magnesia of the experimentally obtained biotites is apparently associated with a partial loss of iron from the melt, which went into the walls of the platinum capsules during the experiments.

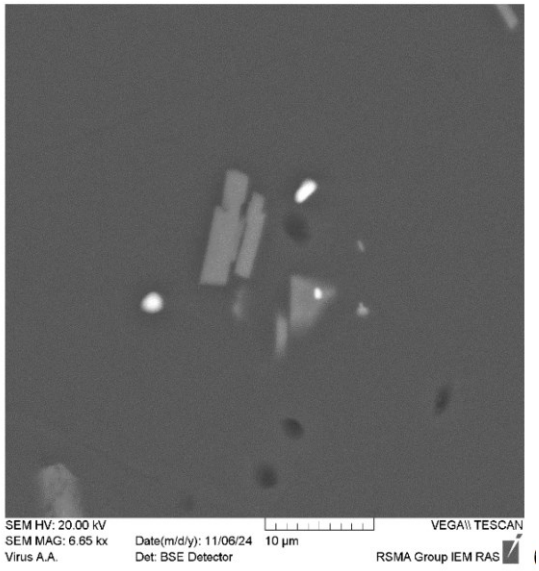

Fig. 2. Biotite crystals crystallizing from the melt.

Table 4. Chemical composition of micas (biotites) obtained in experiments VZ-5/sol and VZ-6/sol (according to EDS data, F and Cl according to wave spectrometer data, in wt. %, normalized to 100 %)

Solution	Experience number	*P*, MPa / *T*, °C	SiO_2	TiO_2	Al_2O_3	FeO_{tot}	MnO	MgO	Na_2O	K_2O	F	Cl	F/Cl	$Mg^{\#}$
Sol-2 – 1M HF + 1M HCl	VZ-5/sol	110/ 720	47.97	2.13	15.47	8.78	0.12	14.16	1.01	7.44	2.47	0.14	17.21	74.51
	VZ-6/sol	315/ 690	46.27	1.89	15.08	9.95	0.09	14.89	0.72	8.40	2.56	0.14	21.61	72.45
Sol-4 – 5M HF + 1M HCl	VZ-5/sol	110/ 720	46.92	1.33	14.37	7.47	0.10	15.81	0.99	7.89	4.98	0.13	40.32	78.83
	VZ-6/sol	315/ 690	48.04	1.44	13.37	7.43	0.11	14.96	1.02	8.40	5.13	0.09	60.24	79.36

$Mg^{\#}$ - magnesia coefficient equal to the mole ratio 100×Mg/ (Mg+Mn+Fe).

The main results, illustrated by diagrams of the obtained dependencies, are considered in more detail in another report by Chevychelov V.Yu. and Viryus A.A. "Influence of pressure and melt composition on the partition of F and Cl in the biotite – granite melt system".

Funding. *This study is fulfilled under financial support of the project of the Russian Federation represented by the Ministry of Education and Science of Russia, project No. 13.1902.24.44, agreement No. 075-15-2024-641.*

References

Zaraysky G.P. et al. Experimental substantiation of the physico-chemical model of the formation of tantalum deposits associated with lithium-fluoride granites. In: Experimental studies of endogenous processes. In memory of academician V.A. Zharikov. — Chernogolovka: Editorial and Publishing Department of the IPCP of RAS. 2008. — P. 86-109.

Reif F.G. Ore-forming potential of granites and conditions for its implementation. Moscow: Science. — 1990. — 181 p.

Reif F.G., Seltmann R., Zaraisky G.P. The role of magmatic processes in the formation of banded Li-F-enriched granites from the Orlovka tantalum deposit Transbaikalia, Russia: microthermometric evidence // Canadian mineralogist. — 2000. — V. 38. — P. 915-936.

Rieder M. et al. Nomenclature of micas // Mineralogical Magazine. — 1999. — V. 63 (2). — P. 267–279.

Chevychelov V.Y., Viryus A.A. Influence of pressure and melt composition on the

partition of F and Cl in the biotite - granite melt system. *UDC 550.42*

Korzhinskii Institute of Experimental Mineralogy RAS;
chev@iem.ac.ru, allavirus@yandex.ru

Abstract. The partition of F and Cl in the system of biotite crystallizing from melt – granite melt at temperatures of 690 - 760°C in the presence of chloride-fluoride aqueous solutions of different concentrations was experimentally studied. In order to assess the effect of pressure on the compositions of biotite and melt, the experiments were carried out in a wide range of pressures from ~ 100 to ~ 500 MPa. After experiments with 1M HF + 1M HCl solution, the melt contained 0.25-0.35 wt. % F and 0.12-0.23 wt. % Cl, and after experiments with 5M HF + 1M HCl solution, it contained 0.99-1.33 wt. % F and 0.12-0.23 wt. % Cl.

It was found that the F content in mica is significantly higher than in the coexisting granite melt. With increasing pressure, the fluorine content in the melt increases significantly, while in biotite the increase in the F content is more weakly expressed. Chlorine behaves differently in the system under consideration: its content in mica at a pressure of 110 MPa is always lower than in the coexisting granite melt. And with an increase in pressure to 315 MPa, the Cl contents in mica and the melt become close. The F/Cl ratio in the biotite is always higher than in the granite melt. This ratio in the biotite significantly increases both with increasing pressure and with an increase in the fluorine content in the melt. The probable contents of F, Cl and the F/Cl ratio in the granite melt of the Khangilai massif are estimated. The fluorine and chlorine contents in the granite melt were a few hundredths of a percent, 0.0n wt. %, for each element (no more than 0.10-0.15 wt. %), and the F/Cl ratio could vary from 1 to 5 depending on the pressure.

***Keywords**: volatile components partition; fluorine; chlorine; biotite; granite melt composition; pressure; experiment*

Introduction to the topic, the methodology of the conducted research and the main results, in the form of tabular data, are given above in another report by Chevychelov V.Yu. and Viryus A.A. “Study of F and Cl partition between biotite crystallizing from melt and granite melt at subliquidus conditions”.

Main results. It was established that F, Cl-containing biotites crystallized in the presence of F, Cl-containing and Cl-containing fluids (1M HF + 1M HCl, 5M HF + 1M HCl, 0.33M HCl + 0.33M NaCl + 0.33M KCl; with a content of 0.12-0.23 wt. % Cl in the glass), but only at the pressure of 110 and 315 MPa.

In the presence of fluoride fluid (2M HF + 2M KF) and pure H_2O, F-containing biotite was formed, the Cl content of which was near the detection limit. This F-containing biotite crystallized in the entire studied pressure range from 110 to 535 MPa, but the higher the pressure in the experiment, the smaller the size and number of biotite crystals.

In the presence of concentrated fluid (5M HF + 5M HCl), biotite did not crystallize at all (with the glass content of 1.08 wt. % F and 0.54 wt. % Cl).

In synthesized biotites, a negative correlation is observed between the contents of F in mica on the one hand, and Fe and Ti on the other hand. For example, with a decrease in F content from 4.55 to 1.11 wt. %, the FeO content increases from 5.40 to 11.47 wt. %, and the TiO_2 content from 1.82 to 2.83 wt. %.

It has been established that the fluorine content in mica is significantly higher than in the granite melt coexisting with it (Fig. 1). With increasing pressure, the fluorine content in the melt increases noticeably, while in biotite the increase in the F content is less pronounced.

Chlorine behaves in other way in the system under consideration: its content in mica at pressure of 110 MPa is always lower than in the coexisting granite melt. And with increase in pressure to 315 MPa, the Cl contents in mica and melt become close (Fig. 2). Thus, with increase in pressure, the chlorine content in the melt decreases and decreases more noticeably compared to the decrease in Cl in biotite.

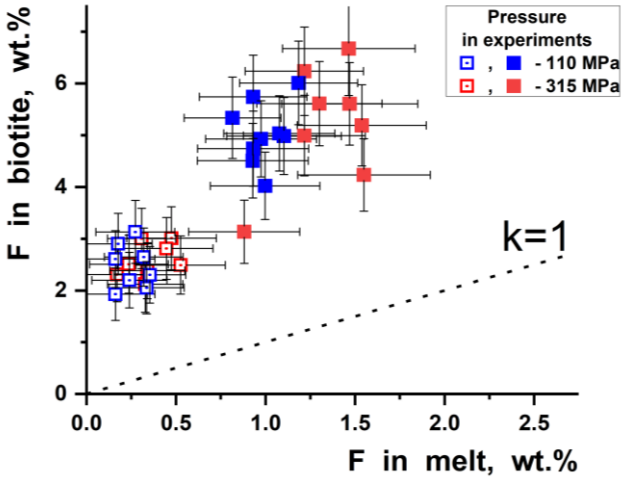

Fig.1.

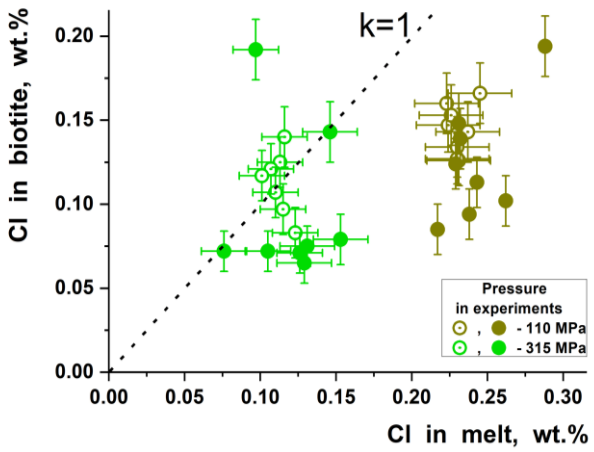

Fig.2.

Fig. 1. Dependence of the F content in biotite on the F content in granite melt at subliquidus conditions. *Unfilled symbols* indicate that the melt contained 0.25-0.35 wt. % F and 0.12-0.23 wt. % Cl, *filled symbols* indicate that the melt contained 0.99-1.33 wt. % F and 0.12-0.23 wt. % Cl. The dotted line (k = 1) corresponds to the equality of fluorine contents in mica and in the melt.

Fig. 2. Dependence of Cl content in biotite on Cl content in granite melt. *Unfilled symbols* indicate melt contained 0.25-0.35 wt. % F and 0.12-0.23 wt. % Cl, *filled symbols* indicate melt contained 0.99-1.33 wt. % F and 0.12-0.23 wt. % Cl. Dotted line (k = 1) corresponds to equal chlorine content in mica and melt.

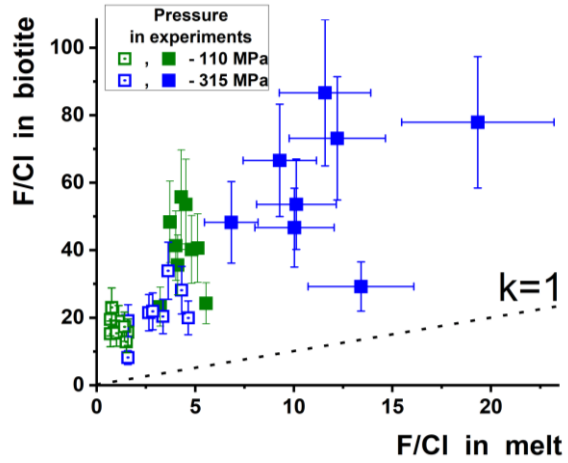

Fig. 3. Dependence of the F/Cl ratio in the biotite on the F/Cl ratio in the coexisting granite melt. *Unfilled symbols* indicate that the melt contained 0.25-0.35 wt. % F and 0.12-0.23 wt. % Cl, *filled symbols* indicate that the melt contained 0.99-1.33 wt. % F and 0.12-0.23 wt. % Cl. The dotted line (k = 1) corresponds to the equality of fluorine contents in mica and in the melt.

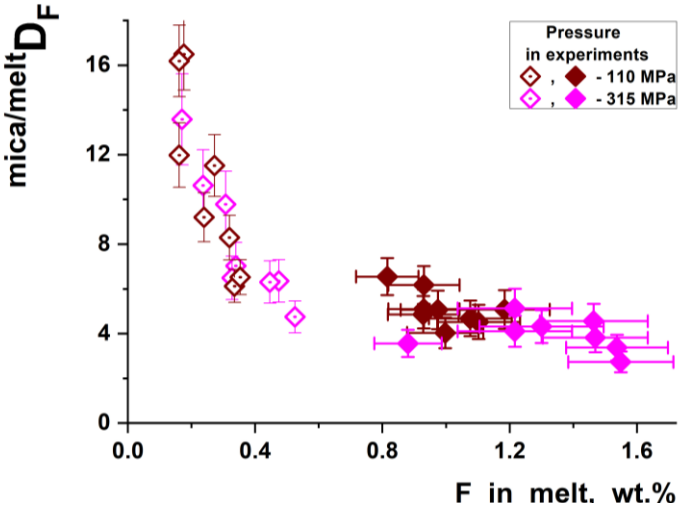

Fig. 4. Dependence of the partition coefficient of F between mica and melt on the F content in the granite melt. *Unfilled symbols* indicate that the melt contained 0.25-0.35 wt. % F and 0.12-0.23 wt. % Cl, *filled symbols* indicate that the melt contained 0.99-1.33 wt. % F and 0.12-0.23 wt. % Cl.

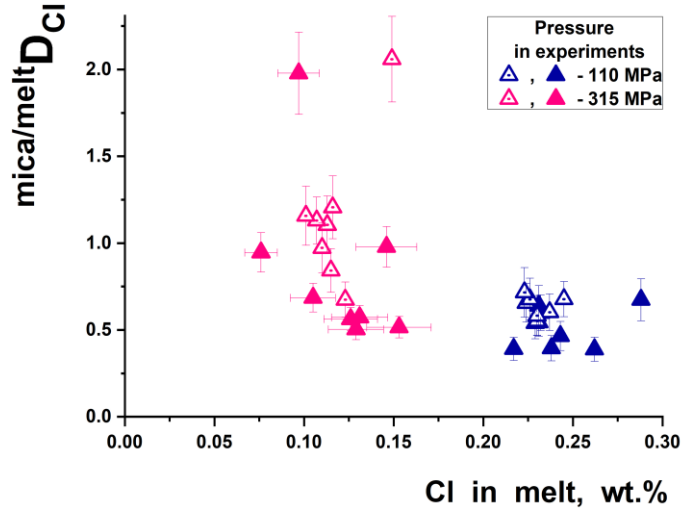

Fig. 5. Dependence of the Cl partition coefficient between mica and melt on the Cl content in the granite melt. *Unfilled symbols* indicate that the melt contained 0.25-0.35 wt. % F and 0.12-0.23 wt. % Cl, *filled symbols* indicate that the melt contained 0.99-1.33 wt. % F and 0.12-0.23 wt. % Cl.

The F/Cl ratio in biotite is always higher than in granite melt (Fig. 3). This ratio in biotite increases significantly with both increasing pressure and increasing fluorine content in the melt.

The partition coefficient of fluorine between mica and melt decreases with increasing pressure and with increasing fluorine content in the melt (Fig. 4).

The partition coefficient of chlorine between mica and melt changes in other way (Fig. 5). It increases with increasing pressure, but decreases slightly with increasing fluorine content in the melt. The chlorine content in the melt decreases sharply with increasing pressure.

By comparing the experimentally obtained data on the composition of the synthesized biotites and coexisting granite melts with the composition of natural biotite 1 from the granites of the Khangilai massif, the probable contents of F, Cl and the F/Cl ratio in the granite melt of the Khangilai massif were estimated. The contents of fluorine and chlorine in the granite melt were a few hundredths of a percent, 0.0n wt. %, for each element (no more than 0.10-0.15 wt. %), and the value of the F/Cl ratio could vary from 1 to 5 depending on the pressure.

Funding. *This study is fulfilled under financial support of the project of the Russian Federation represented by the Ministry of Education and Science of Russia, project No. 13.1902.24.44, agreement No. 075-15-2024-641.*

Gnuchev Y.Y., Bychkov D.A., Koptev-Dvornikov E.V. An improved equation for calculating the solubility limit of water in silicate melts depending on intensive parameters. *UDC 552.112*

Lomonosov Moscow State University, Geological Faculty, 119234 *Russian Federation, Moscow, GSP-1, Leninskie Gory, gnuchevyakov@mail.ru, dmibychkov@gmail.com, ekoptevmail@gmail.com*

Abstract: Experience in using the previously obtained equation, which allows predicting the value of the limiting solubility of water in a silicate melt, showed that for a number of experiments performed in the pressure range from 10 to 20 kbar, the calculated water contents are unrealistically high compared to the experimental values.

The sample used in the previous work (containing the results of 412 experiments) was significantly supplemented by experiments from the MELT database, kindly provided by A.V. Girnis, and other literary sources.

Based on the newly collected total sample, consisting of 1241 experiments, the set of variables responsible for the effect of composition on water solubility was revised. The newly calibrated equation for calculating the limiting solubility of water allows with an uncertainty not exceeding ±0.01 mole fraction, or ±0.25 wt. % predict saturated water contents in silicate melts in the ranges: pressure from atmospheric to 20 kbar; temperatures from 825 to 1550 K, and the sample size used for optimization allows the equation to be used to calculate saturated water contents in a wide range of silicate melts, from komatiite basalts to rhyolites.

Keywords*: Water solubility model; sample of water-saturated experiments; silicate melt; volatile components*

At present, our research group has developed a set of compositometers (Aryaeva et al., 2016; Bychkov 2024; Koptev-Dvornikov et al., 2012, 2019, 2020; Romanova et al., 2020), which allows predicting the crystallization of olivine, plagioclase, augite, orthopyroxene and ore minerals (sulfides, chromospinelides, magnetite and ilmenite) coexisting with the melt. However, these equations were obtained by processing the results of anhydrous experiments, while the vast majority of natural magmas and lavas are more or less hydrous. Thus, an urgent task is to develop compositometers that are uniform for anhydrous and hydrous systems. When creating the corresponding samples, it turned out that only for 20% of the experiments characterized by the authors as water-saturated, the concentration of water in the melt is given (Ariskin et al., 1996). This excludes 80% of the data from statistical processing, which significantly reduces the quality of the compositometers. In addition, it is necessary to know the limit of water content in the melt, above which water forms an independent vapor phase.

A way out of this situation is to develop an equation that allows calculating the saturated concentration of water in the melt.

In this regard, we previously developed such an equation based on 412 experiments from the INFOREX database (Ariskin et al., 1996) (Gnuchev et al., 2023).

Experience in applying our equation showed that for a number of experiments performed in the pressure range from 5 to 15 kbar, the calculated water contents are unrealistically high. The reason for this is the extremely limited number of experiments in the sample characterizing the pressure range from 5 to 15 kbar (14 experiments in total). Therefore, it made sense to collect a sample of a larger volume of experimental data and, on its basis, return to revising the type of equation and recalibrating it.

Thanks to the kindness of A.V. Girnis, who provided us with the MELT database (Girnis, 2023), as well as the literature found, the sample has significantly expanded from 412 experiments to 1241 experiments, of which 145 experiments were performed at pressures from 5 to 20 kbar, on the basis of which the equation was calibrated, applicable in a wider range of intensive parameters (composition, temperature and pressure). The polyhedron of 1241 experimental melt compositions in oxide concentration coordinates for the newly formed sample is characterized by the following

values (wt. % of oxide content in the melt, recalculated to anhydrous basis): SiO_2 from 43.7 to 80.3, TiO_2 from 0 to 4.9, Al_2O_3 8.9–24.8, FeO* 0–14.9 (FeO* is all iron, recalculated to FeO), MgO 0–20.5, CaO from 0–24.6, Na_2O 0–13.0, K_2O 0–16.8, H_2O 0–17.0. The experiments were performed in the temperature range from 825 to 1550 K and pressures from 1 bar to 20.0 kbar. The distribution of experiments by composition is shown in Fig. 1. The color shows the distribution of experiments in the sample by pressure ranges. Most of the water-saturated experiments are in the range from 0.001 to 2 kbar (759 experiments), some are in the range from 2 to 5 kbar (390), 57 are in the range from 5 to 10 kbar, and 35 experimental points are in the range from 10 to 20 kbar. In contrast to the 2023 sample, the number of experiments performed from 5 to 20 kbar increased from 14 to 145.

Analysis of results. Based on the collected sample, the 2023 equation was recalibrated to:

$$LnX_{H_2O}^{melt} = \frac{a}{T} + b_{SiO_2}X_{SiO_2}\left(\frac{P}{T}\right) + b_{\mathrm{FeO}}X_{\mathrm{FeO}}\left(\frac{P}{T}\right) + cLnP + d \quad (1),$$

where $X_{H_2O}^{melt}$ – saturated mole fraction of water in the melt; T is the temperature in degrees Kelvin; Xi is the mole fraction of oxide in the melt; P is the pressure in bars; a, bi, c are the coefficients of the corresponding variables; d is a constant.

A comparison of the experimental and calculated saturated water contents using the new equation is shown in Fig. 2, and the values of the coefficients are shown in Table 1. The high quality of reproduction of the experimental data is evidenced by the proximity of the angular coefficients in the regression equations to one, the free terms to zero, the values of the determination coefficients close to one, and the very small width of the confidence corridor at the 95% confidence level.

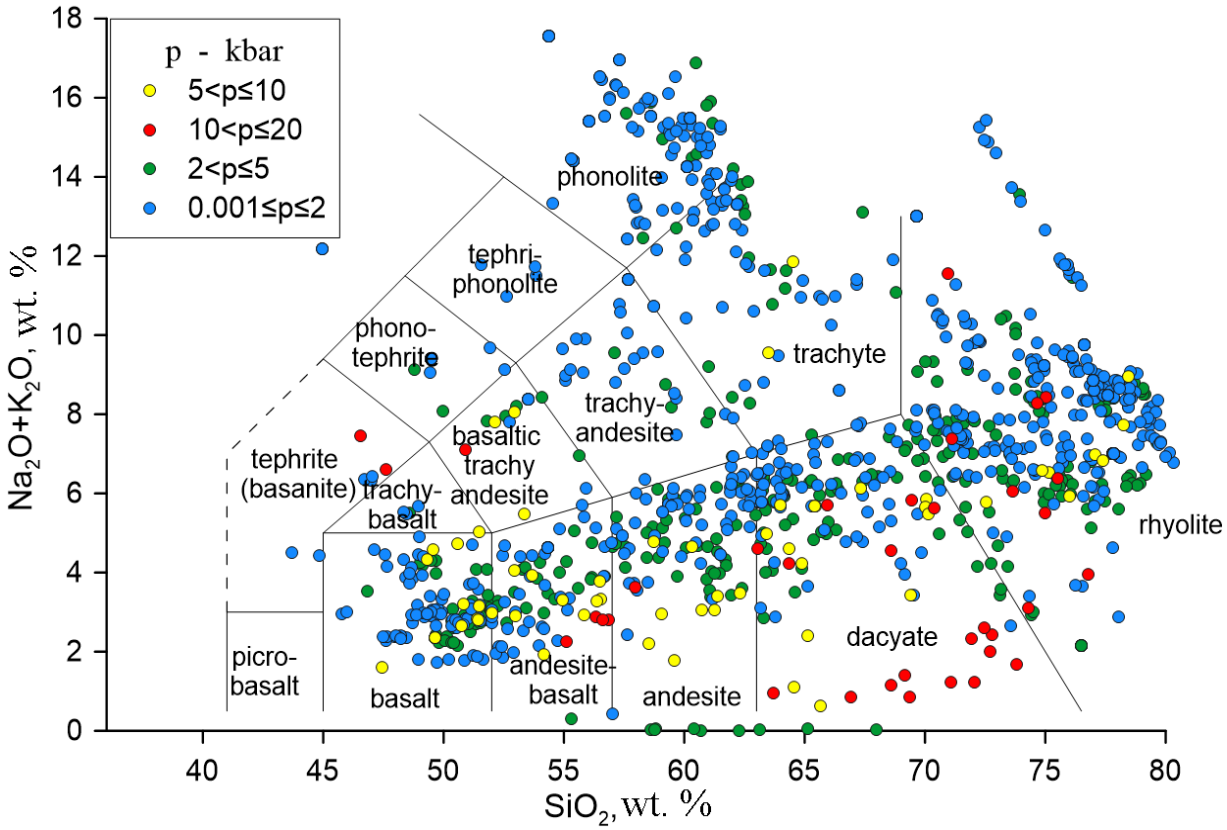

Fig. 1. TAS diagram. Range of variation of experimental melt compositions (1241 experiments in the sample).

Table 1. Values of the coefficients for the variables in equation (1), obtained as a result of data optimization on a sample of 1241 experiments (± is the value of the confidence interval at the 95% confidence level)

	a	b_{SiO2}	b_{FeO}	c	d
wt. %	958.2	-0.000334	-0.00387	0.563	-3.25
±	113.6	0.000077	0.0011	0.0094	0.119

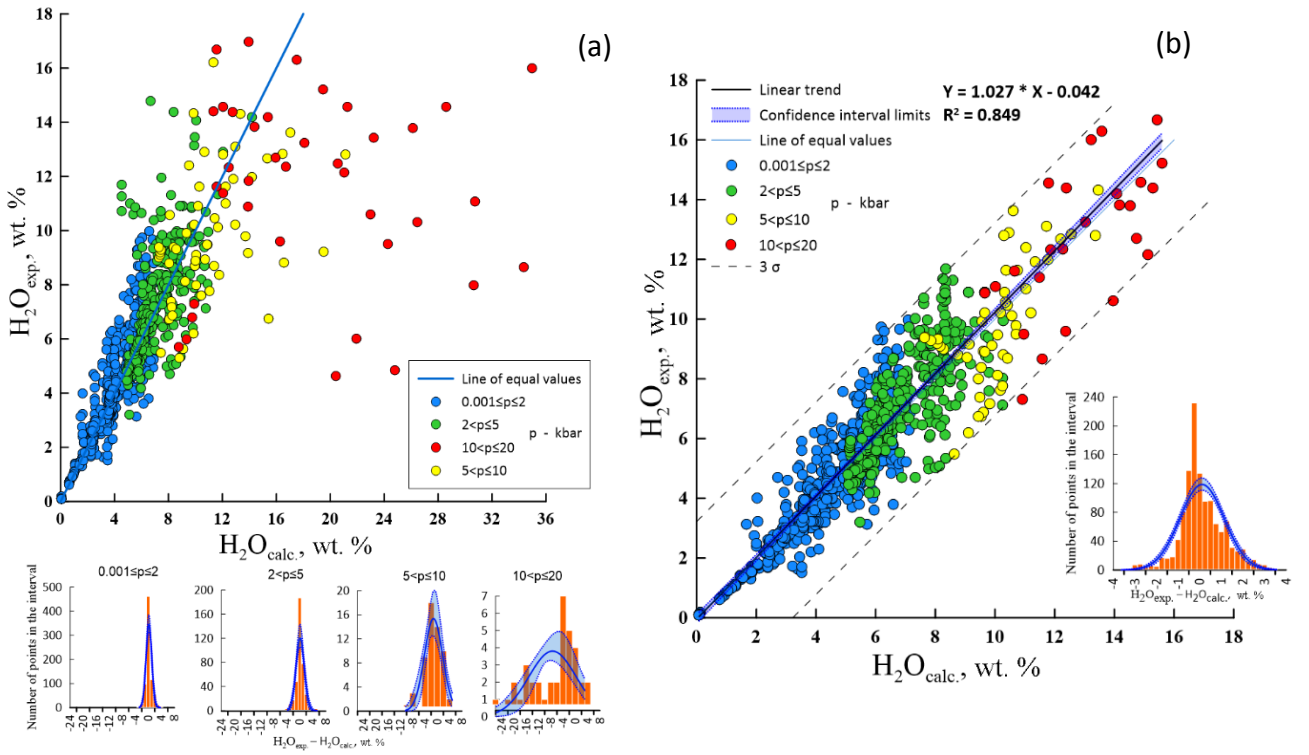

Fig. 2. Comparison of calculated and experimental values of water solubility according to a – the 2023 equation, b – the equation optimized on the general sample (1241 experiments), with experimental data, where the limiting solubility of water is expressed in – wt.%.

As a result of re-optimization of the equation on the new sample, it became possible to predict the limiting solubility of water in a wider range of compositions and pressures than before, up to 20 kbar. This allows using the equation:

– when planning experiments and checking the realism of the results obtained;
– to determine the conditions for separating aqueous fluid from evolving magma in the intermediate chamber of a volcano or intrusion chamber;
– to expand the samples used to derive compositometers-thermobarometers (systems of equations simulating mineral-melt equilibrium).
– the presence of such an equation will solve the problem of the limited sample size of water-containing experiments when optimizing the equations of thermobarometers.

Conclusions

- A new sample of water-saturated experimental data has been collected, which has increased by more than 3 times compared to the previous one (up to 1241 experiments). The range of intensive parameters has been expanded.
- Based on the new sample, an equation has been optimized that reproduces the experimental data significantly better than before, especially in the pressure range from 5 to 20 kbar. With a probability of 95%, the calculated saturated water content in the silicate melt differs from the true one by no more than ±0.01 mole fraction, or ±0.25 wt. %.

Acknowledgments

The authors express their sincere gratitude to the teams led by A.V. Girnis and A.A. Ariskin for providing the MELT and INFOREX databases, which significantly simplified the search and evaluation of the necessary works.

References

Aryaeva N. S., Koptev-Dvornikov E. V., Bychkov D. A. Thermobarometer equation for describing sulfide-silicate liquation in basic systems // Petrology. - 2012. - Vol. 20. - No. 5. - P. 495-495.

Ariskin A. A. et al. INFOREX-3.0: A database on experimental studies of phase equilibria in igneous rocks and synthetic systems: II. Data description and petrological applications // Computers & Geosciences. - 1996. - Vol. 22. - No. 10. - P. 1073-1082.

Bychkov D. A. The CriMinal program and a set of composite meters: tools for modeling the silicate melt – mineral equilibrium, Dis. Cand. Geol.-Min. Sciences. Moscow: Lomonosov Moscow State University, Geological Faculty, 2023. – p. 139.

Girnis A.V. (2023) Distribution of rare elements between olivine and melt: generalization of experimental data// Geohimiâ. – 2023. – Vol. 68. – No. 4. – P. 327-340.

Gnuchev Ya. Yu., Bychkov D. A., Koptev-Dvornikov E. V. New version of the equation for calculating saturated water contents in silicate melts // Geohimiâ. – 2023. – Vol. 68. – No. 9. – P. 926-937.
Koptev-Dvornikov E. V., Aryaeva N. S., Bychkov D. A. Thermobarometer equation for describing sulfide-silicate liquation in basic systems // Petrology. - 2012. - Vol. 20. - No. 5. - P. 495-495.
Koptev-Dvornikov E. V., Bychkov D. A. (2019) Development of a liquidus thermobarometer for modeling olivine-melt equilibrium. Bulletin of Moscow University. Series 4: Geology. (5), 62-74.
Koptev-Dvornikov E. V., Romanova E. S., Bychkov D. A. Orthopyroxene liquidus thermobarometer-composiometer for the range of melt compositions from magnesian basites to dacites // Proceedings of the All-Russian annual seminar on experimental mineralogy, petrology and geochemistry. - 2020. - pp. 74-77.
Romanova E. S., Koptev-Dvornikov E. V., Bychkov D. A. Pigeonite liquidus thermobarometer for the range of melt compositions from magnesian basites to dacites // Proceedings of the All-Russian annual seminar on experimental mineralogy, petrology and geochemistry. - 2020. - P. 90-93.

Korzhinskaya V.S., Suk N.I., Kotelnikov A.R., Novikov M.P., Van K.V. Solubility of $Zr_{0.5}Hf_{0.5}SiO_4$ solid solution in aluminosilicate melt at temperatures of 800 °C, 1000 °C and pressures of 200, 400 MPa. *UDC 550.89*

IEM RAS, Chernogolovka, Moscow region
(vkor@iem.ac.ru)

Abstract. Experimental data on the solubility of the $Zr_{0.5}Hf_{0.5}SiO_4$ solid solution in an aluminosilicate melt at temperatures of 800°C and 1000°C for pressures of 200 and 400 MPa in dry conditions and in the presence of water are obtained. The starting material was fused granite glass of different agpaiticity, as well as a solid solution of the composition: $Zr_{0.5}Hf_{0.5}Si0_4$, synthesized by the solution-melt method. It has been established that in water-containing melts, with increasing agpaiticity, the content of Σ (ZrO_2+HfO_2) in the glass increases. Under dry conditions, a halo with increased alkalinity and increased content of (ZrO_2 + HfO_2) is formed around the $Zr_{0.5}Hf_{0.5}SiO_4$ crystals. Under the studied parameters, the formation of alkali zirconium silicate crystals is observed in the glass.

***Keywords**: aluminosilicate melt, solid solution, experiment, solubility, zirconium, hafnium*

Experimental data on the solubility of the $Zr_{0.5}Hf_{0.5}SiO_4$ solid solution in an aluminosilicate melt were obtained for temperatures of 800 and 1000 °C and pressures of 200 and 400 MPa. The experiments were carried out on a high gas pressure vessel (HGPV-10000) in the presence of water and under dry conditions. The duration of the experiments was 12 days for 800 °C and 5 days for 1000 °C. The starting material was fused granite glass of different agpaiticity (Kagp = (Na + K) / Al): 0.95 - 2.05, as well as a solid solution of the $Zr_{0.5}Hf_{0.5}Si0_4$ composition, synthesized by the solution-melt method (Kotelnikov et al., 2023). The composition of the samples after the experiments was determined by the method of electron probe X-ray spectral analysis.

The experimental method for determining the effect of agpaiticity on the solubility of $Zr_{0.5}Hf_{0.5}SiO_4$ (ZrcHfn) was described by us earlier (Kotelnikov et al., 2019). A similar method was used to study the solubility of the $Zr_{0.5}Hf_{0.5}SiO_4$ solid solution in an aluminosilicate melt in the presence of water and under dry conditions. The experiments were carried out in gold (800°C) and platinum (1000°C) ampoules 3x0.1x50 mm, and 4x0.1x50, into which 50-80 mg of granite glass and 5-7 mg of the synthesized $Zr_{0.5}Hf_{0.5}SiO_4$ solid solution were loaded. If necessary, a certain amount of water was poured into the ampoules. The ampoules were hermetically sealed and placed in a “gas” bomb to conduct the experiment. The compositions of all samples after the experiments were determined by the method of electron probe X-ray spectral analysis (EPXRSA) using a Tescan Vega II XMU scanning electron microscope (Tescan, Czech Republic), equipped with an INCA Energy 450 X-ray spectral microanalysis system with energy-dispersive (INCAx-sight) and crystal diffraction (INCA wave 700) X-ray spectrometers (Oxford Instruments, England) and the INCA Energy+ software platform.

The results of experiments in hydrous melts were described by us earlier (Kotelnikov et al., 2023; Korzhinskaya et al., 2024). In this paper, the results of the behavior of the $Zr_{0.5}Hf_{0.5}SiO_4$ solid solution in a dry system are presented. Tables 1 and 2 present the results of experiments on the solubility of $Zr_{0.5}Hf_{0.5}SiO_4$ in a melt with different agpaiticity under dry conditions at T = 800° and 1000°C, P = 400 MPa, and Fig. 1 shows the curves of the dependences of the solubility of ZrcHfn in an aluminosilicate melt on the agpaiticity Kagp in a dry system for temperatures of 1000°C and 800°C. For comparison, Fig. 2 shows the solubility curves of the solid solution in the presence of water for the same parameters. It was found that the solubility of ZrcHfn depends on the composition of the aluminosilicate melt, increasing with increasing its agpaitic ratio (Na+K)/Al in both the aqueous and dry systems.

For T = 800 °C and P = 400 MPa, in addition to the aluminosilicate glass, in which the contents of (ZrO_2+HfO_2) are practically absent, a silicate glass of increased alkalinity with a high content of sodium and (ZrO_2+HfO_2) is also formed. Photo 1 shows the formation of glasses with different alkalinity (L1 and L2) in a dry system. L1 is an aluminosilicate glass

with Kagp aft/exp = 4.30. The composition of glass L1 after the experiment is as follows (wt. %): Na_2O – 9.18; Al_2O_3 – 4.86; SiO_2 – 65.88; K_2O – 3.78; CaO – 0.43; TiO2 – 0.10; MnO – 0.32; FeO – 1.05; (ZrO_2+HfO_2) – 14.93. L2 – aluminosilicate glass; Kagp aft/exp = 1.15. The composition of glass L2 is as follows (wt. %): Na_2O – 6.15; Al_2O_3 – 14.05; SiO_2 – 73.36; K_2O – 5.50; FeO – 0.26; (ZrO_2+HfO_2) – absent.

Table 3 presents the results of experiments on the solubility of $Zrc_{0.5}Hfn_{0.5}Si0_4$ in the melt under dry conditions for different initial agpaiticity (Kagp befor/exper = 1.30; 2.05 and 2.50) at T = 800°C and P = 200 MPa. At these parameters, a halo of glass with increased alkalinity enriched in (ZrO_2+HfO_2) is formed around the ZrcHfn crystals, as well as the formation of new small crystals of alkali zirconium silicates. In Photo 2, L1 is a halo of glass with increased alkalinity around the crystals of the ZrcHfn solid solution. (Kagp befor/exper. = 2.05; Kagp after/exper. = 3.68). The composition of the glass is as follows (wt. %): Na_2O – 9.46; Al_2O_3 – 4.99; SiO_2 – 59.28; K_2O – 4.01; (ZrO_2+HfO_2) – 10.74. Under dry conditions, crystals of alkali zirconium silicate (NZHS, see photo 2) with the formula $Na_{4.7}(Zr,Hf)_{2.76}Si_{7.8}O_{15.85}$ are formed around the crystals of the ZrcHfn solid solution.

Table 1. Experiments on the solubility of $Zr_{0.5}Hf_{0.5}Si0_4$ in a melt with different agpaitic values in a dry system for T = 800 °C, and P = 400 MPa

№ exp	Weight, mg	Solution, mg	ZrO_2, wt.%	HfO_2, wt.%	ZrcHfn, wt.%	Kagp befor/exp Kagp after/exp
ZrcHfn-34	58.20gr.+3.04 $Zrc_{0.5}Hfn_{0.5}$	Dry system	6.51	13.00	19.51	Kagp bef/ex=1.51 Kagp aft/ex =6.62
ZrcHfn-32	56.11gr.+5.09 $Zrc_{0.5}Hfn_{0.5}$	Dry system	5.29	9.64	14.93	Kagp bef/ex=1.19 Kagp aft/ex =4.30
ZrcHfn-36	58.20gr.+3.04 $Zrc_{0.5}Hfn_{0.5}$	Dry system	4.31	9.53	13.83	Kagp bef/ex=1.30 Kagp aft/ex=3.87
ZrcHfn-38	83.51gr.+9.35 $Zrc_{0.5}Hfn_{0.5}$	Dry system	3.03	5.40	8,43	Kagp bef/aft=2.05 Kagp bef/ex=4.88

Note: gr. –granite glass

Table 2. Experiments on the solubility of $Zr_{0.5}Hf_{0.5}Si0_4$ in a melt with different agpaitic values in a dry system for T = 1000 °C, and P = 400 MPa

№ exp	Weight, mg	Solution, mg	ZrO_2, wt.%	HfO_2, wt.%	ZrcHfn, wt.%	Kagp befor/exp Kagp after/exp
ZrcHfn-29	53.66gr.+67.29 $Zrc_{0.5}Hfn_{0.5}$	Dry system	2.51	4.61	7.12	Kagp bef/ex=1.51 Kagp aft/ex=1.75
ZrcHfn-30	56.07gr.+5.23 $Zrc_{0.5}Hfn_{0.5}$	Dry system	3.89	6.52	10.41	Kagp bef/ex=2.05 Kagp aft/ex=2.21

Note: gr.- granite glass

Table 3. Experiments on the solubility of $Zr_{0.5}Hf_{0.5}Si0_4$ in a melt with different agpaitic values in a dry system for T = 800 °C, and P = 200 MPa

№ exp	Weight, mg	Solution, mg	ZrO_2, wt.%	HfO_2, wt.%	ZrcHfn, wt.%	Kagp befor/exp Kagp after/exp
ZrcHfn-39	53.38gr.+7.81 $Zrc_{0.5}Hfn_{0.5}$	Dry system	6.07	11.26	17.33	Kagp bef/ex=1.30 Kagp aft/ex = 3.68
ZrcHfn-40	50.56gr.+8.31 $Zrc_{0.5}Hfn_{0.5}$	Dry system	3.59	7.15	10.74	Kagp bef/ex=2.05 Kagp aft/ex=3.68
ZrcHfn-41	52.17gr.+7.70 $Zrc_{0.5}Hfn_{0.5}$	Dry system	3.80	6.50	10.30	Kagp bef/ex=2.50 Kagp aft/ex=3.37

Note: gr. –granite glass

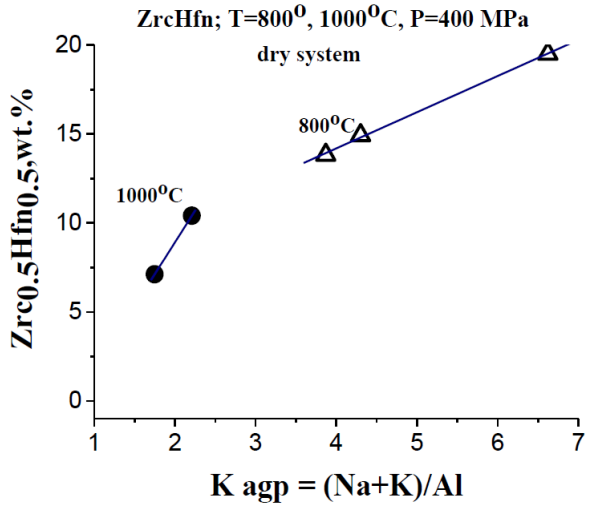

Fig. 1. Curves of the dependences of the solubility of $Zrc_{0.5}Hfn_{0.5}$ in an aluminosilicate melt on the agpaiticity Kagp in a dry system

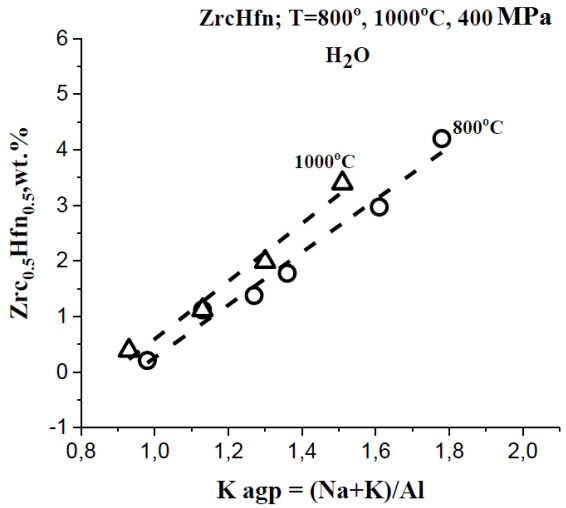

Fig. 2. Curves of the dependence of the solubility of $Zrc_{0.5}Hfn_{0.5}$ in an aluminosilicate melt on the agpaiticity Kagp in a water-containing system

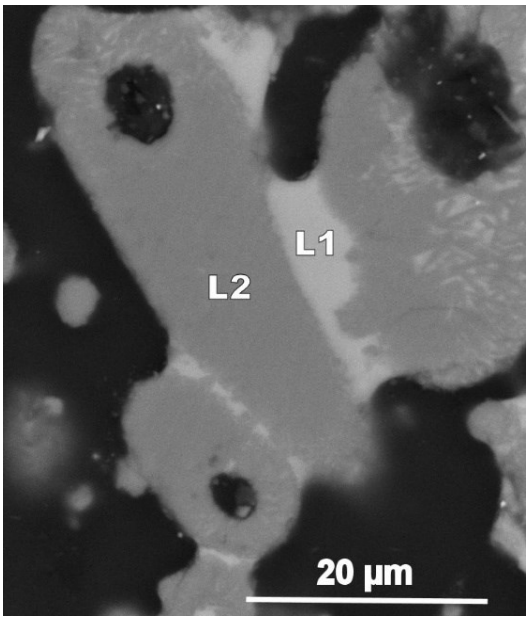

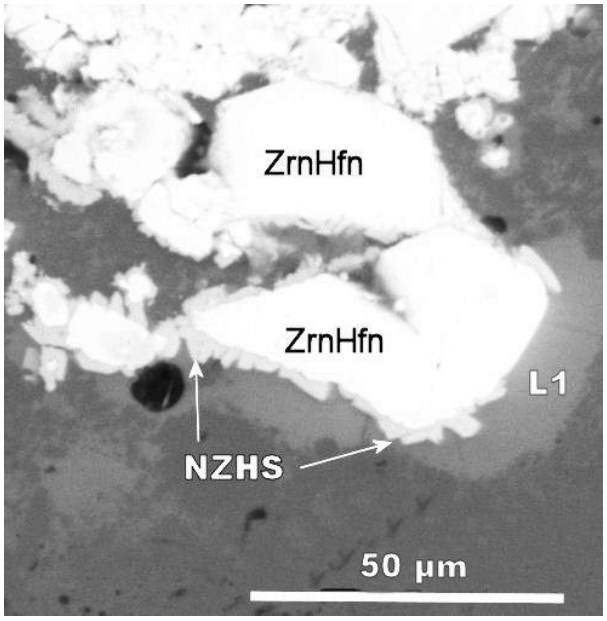

Photo 1. Formation of glasses with different alkalinity (L1 and L2) in a dry system at T = 800 °C and P = 400 MPa (sample ZrcHfn-32; Kagp befor/exper. = 1.2)

Photo 2. Formation of a halo of glass with increased alkalinity, as well as new crystals of alkali zirconium silicates. Sample ZrcHfn – 40. T = 800°C, P = 200 MPa (dry system). NZHS – alkali zirconium silicates.

The work was supported by a grant from the Ministry of Education and Science of Russia for the implementation of scientific project 13.1902.24.44 (23-075-67362-1-0409-000006).

References

Kotelnikov A.R., Korzhinskaya V.S., Suk N.I., Van K.V., Virus A.A. Experimental study of zircon and loparite solubility in silicate melt // Experiment in Geosciences, 2019, Volume 25, N 1, P.P.138 - 140. (ISSN: 0869-2904).

Kotelnikov A.R., Korzhinskaya V.S., Suk N.I., Novikov M.P., Van K.V. Experimental investigation of solubility of $Zr_{0.5}Hf_{0.5}SiO_4$ solid solution in silicate melts. // Experiment in Geosciences, 2023, Volume 29, N 1, P.P.153 - 155. (ISSN: 0869-2904).

Korzhinskaya V.S., Kotelnikov A.R., Suk N.I., Van K Experimental investigation of solubility of $Zr_{0.5}Hf_{0.5}SiO_4$ solid solution in silicate melts (T = 800°, 1000°C, P – 400 MPa) // Experiment in Geosciences, 2024, Volume 29, N 1, P.P.153 - 155. (ISSN: 0869-2904).

Persikov E.S.[1], Bukhtiyarov P.G.[1], Aranovich L.Ya.[2,1], Sultanov D.M.[1], Shaposhnikova O.Yu.[1] , Nekrasov A.N.[1] **Some features of the interaction process in the basalt melt - methane-hydrogen fluid system at moderate pressures (preliminary results).**

[1]- IEM RAS; [2] IGEM RAS

Abstract: This paper presents the first results of experimental modeling of the formation of native metals (Fe, Ni, Co) in the Earth's crust during the interaction of basalt melts with fluid (H_2+ CH_4) at temperatures (1100 - 1250 °C) and fluid pressures (10-100 MPa) under strongly reducing conditions $f(O_2)=10^{-12}$-10^{-14} MPa. Based on experimental modeling, the following features of the interaction of the reducing fluid with basalt melts have been established: 1. Despite the high reduction potential of the (H_2 + CH_4) + magmatic melt system, the reactions of hydrogen oxidation and complete reduction of metal oxides of variable valence in the melt do not proceed to the end. The cessation of redox reactions in the basalt melt occurs due to the formation of H_2O in the melt, buffering the reduction potential of the fluid (H_2+ CH_4). 2. The complex process of metal-silicate liquation in magmatic melts during their interaction with the reducing fluid can be carried out at real temperatures of magmas in nature (≤ 1250 °C). 3. Carbon, which is formed in experiments due to pyrolysis of CH_4, is dissolved in the metallic phase. Thus, the mechanism responsible for the presence of carbon in native iron in nature has been experimentally substantiated.

Keywords*: basalt, melt, hydrogen + methane, pressure, temperature, native metal, liquation, reducing conditions*

The iron boulders discovered at the end of the 19th century on the southwest coast of Disko Island (Western Greenland) were initially described as meteorites. However, further research has led to the conclusion of their earthly origin. Iron xenoliths in the basalt of Disko Island were most likely transported to the surface along with the erupted basalt (Bird et al.; et al.). In Russia, large-scale manifestations of native iron were found in the Arctic, in the north of the Krasnoyarsk Territory, in the trap intrusions of Dzhaltulsky, Khungtukunsky, Khinindinsky and Maymechinsky (Oleinikov et al., 1985; Ryabov et al., 1985; Tomshin et al., 2023; et al.). Native iron forms nodular segregations in which cogenite, troilite, and magnetite-wustite are present in subordinate amounts. Ni, Co, Au, and PGE are actively concentrated in metallic iron. It has been found that their content in the metal increases hundreds and even thousands of times compared to the host silicate rock (Tomshin et al., 2023). According to Yakut geologists, the formation of native iron is based on the fluid-magmatic interaction of magma matter with the reducing components of the fluid, mainly of methane-hydrogen composition (Oleinikov et al., 1985; Tomshin et al., 2023; et al.). This paper presents the first results of experimental modeling of the formation of native metals (Fe, Ni, Co) in the Earth's crust during the interaction of basalt melts with fluid (H_2+CH_4) at temperatures (1100 - 1250 °C) and fluid pressures (10-100 MPa) under highly reducing conditions $f(O_2)=10^{-12}$-10^{-14} MPa (Table 1).

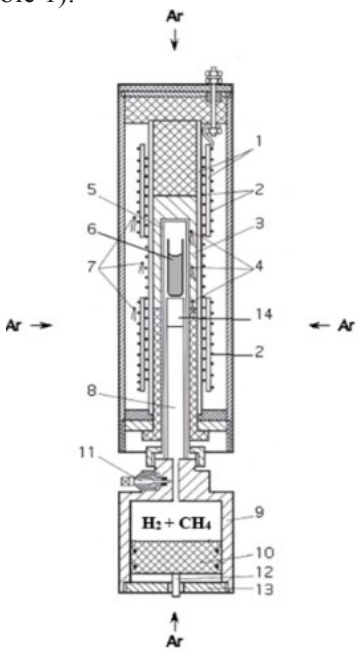

Fig. 1. Diagram of a unique internal device with an internal heater of a high-pressure vessel.
1, 3 - insulators; 2 - two heater windings; 4 - three thermocouples to control the temperature gradient along the sample ampoule; 5 - molybdenum reactor; 6 – alund ampoule with sample (melt); 7 - two thermocouples to control the temperature of each heater winding; 8 - sapphire cylinder; 9 - equalizer housing-separator; 10 – equalizer separator piston; 11 – shut-off valve; 12 - sensor for monitoring the position of the piston; 13 - lid; 14 – alund ampoule with tantalum wire

The experiments were carried out using a unique high-pressure gas installation equipped with an original internal device, which made it possible to conduct long-term experiments at high temperatures, despite the high penetrating power of hydrogen (Fig.1.). The device includes a molybdenum reactor with a molybdenum ampoule containing the initial sample. The reactor is hermetically connected to a piston equalizer separator. The internal volumes of the molybdenum reactor and the equalizer separator under the piston were filled with methane with a hydrogen mixture at a pressure of 10 MPa using a special system. The device assembled in this way, together with an internal heater, was placed inside a high-pressure vessel in such a way that the ampoule with the sample was in a temperature-free zone of the heater. By moving the piston of the equalizer separator, the fluid pressure in the internal volume of the molybdenum reactor was always maintained equal to the gas pressure (Ar) in the vessel during the experiment. The measurement error of the experimental temperature was ± 5 °C, and the

hydrogen pressure was ± 0.1% rel. Natural samples of igneous rocks were used in the experiments: magnesian basalt from the northern eruption of Tolbachik volcano (Kamchatka), as well as magnesian basalt enriched in nickel and cobalt oxides (Table 2). The parameters of the experiments are given in Table 1.

Table 1. Parameters of the conducted experiments and the phases after them

Run number	Fluid	P, MPa	T° C	t, hours	X, H_2O wt. %	Phases	Glass, wt. %		Metal, wt. %	
							SiO_2	FeO	Fe	P
2177	$CH_4 + H_2$ (10 + 90 vol.%)	100	1250	5	0,53	Gl + Me	59,03	1,20	96,84	3,16
2179		100	1250	2	0,42	Gl +Me	56,28	1,78	97,75	2,25
2180		100	1250	2	-	Gl +Me	55,1	3,47	97,77	2,23
2181		100	1250	2	-	Gl +Me	55,63	2,48	97,99	2,01
2182		100	1250	2	-	Gl +Me	55,54	2,76	99,62	0,38

Based on experimental modeling, the following features of the interaction of the reducing fluid with basalt melts have been established:

1. Despite the high reduction potential of the (H_2+CH_4) magmatic melt system, the reactions of hydrogen oxidation and complete reduction of metal oxides of variable valence in the melt do not proceed to the end. The cessation of redox reactions in the basalt melt occurs due to the formation of H_2O in the melt (Table 2), buffering the reduction potential of the fluid (H_2+CH_4).

2. The initially homogeneous magmatic melt becomes heterogeneous: the formed H_2O dissolves in the melt and, partially, in the fluid phase, while melts of a more acidic composition are formed (Table 2) and small metallic separations of the liquation structure (Fig. 2, 6, Table 3).

3. The complex process of metal-silicate liquation in magmatic melts during their interaction with a reducing fluid can be carried out at real temperatures of magmas in nature (≤ 1250 °C), significantly lower than the corresponding melting points of iron and its alloys with nickel and cobalt.

4. Carbon, which is formed in experiments due to pyrolysis of CH_4, dissolves in the metallic phase (Table 3, Fig. 3), thereby experimentally substantiating the mechanism responsible for the presence of carbon in native iron in nature.

5. The structure and dimensions of experimentally established metallic separations are in good agreement with natural data on the finds of native metals, primarily iron and its alloys with nickel and cobalt, in igneous rocks of various compositions and genesis (Fig. 5, 6).

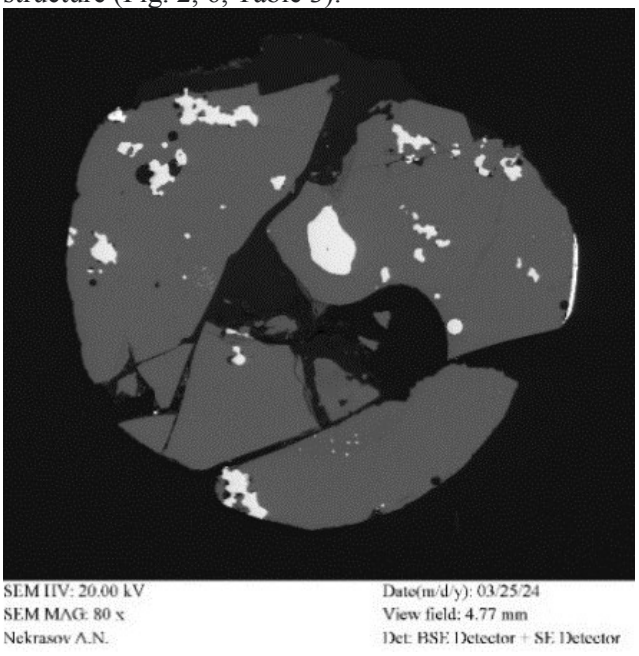

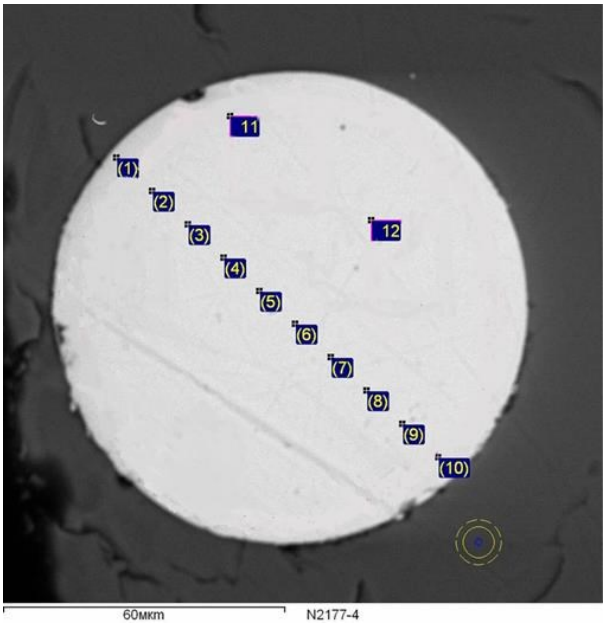

Fig. 2. Backscattered electrons (BSE) image of the products of experiment 2177: white – metallic iron alloy, gray – basalt glass).

Fig. 3. Backscattered electron (BSE) image of the cross-section of a metal ball from experiment 2177. The dots represent the analysis numbers in Table 3

Table 2. Chemical composition (wt.%) and the structural- chemical parameter (100NBO/T) of the initial basalt and basalt glasses after experiments under fluid pressure (10% methane + 90% hydrogen, vol.%)

Oxides	2177* 5 h	2179* 2 h	The composition of the initial basalt (basalt**)
SiO_2	59.03	56.28	49.5
Al_2O_3	15.14	15.20	13.18
Fe_2O_3	0.00	0.00	3.18
FeO	1.20	1.78	6.85
MnO	0.0	0.0	0.15
MgO	7.87	10.14	9.98
CaO	11.08	12.16	12.34
Na_2O	3.00	2.28	2.18
K_2O	1.44	0.93	0.93
TiO_2	1.02	1.18	1.01
P_2O_5	0.02	0.04	0.25
NiO	0.07	0.07	ND
Co_3O_4	0.1	0.1	ND
H_2O^-	0.53	0.42	0.29
Sum	100.33	100.42	99.84
100NBO/T	44.4	62.6	83

Table 3. Composition of the metal phase, wt. %

№ of point	P	Fe	Ni	Co	C**	Sum
1	0.84	96.42	0.11	0.31	2.32	100
2	0.47	98.32	0	0.17	1.05	100
3	0.57	97.04	0.05	0.33	1.01	100
4	0.55	97.35	0	0.21	1.89	100
5	0.71	97.55	0	0.48	1.26	100
6	0.67	97.19	0.11	0.6	1.43	100
7	0.77	96.8	0.06	0.49	1.88	100
8	0.76	96.86	0.13	0.55	1.7	100
9	0.57	98.18	0.22	0.36	0.67	100
10	0.84	97.48	0	0.69	0.99	100
11	1.42	96.6	0.14	0.7	1.15	100
The average values	0.74	97.25	0.07	0.44	1.40	100

*The location of the points is shown in Fig. 3

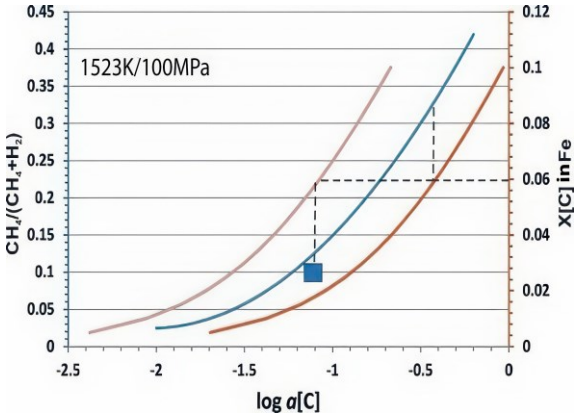

Fig. 4. Curves of the dependence of the composition of the H_2- CH_4 fluid (blue, blue ordinate scale) and the activity-composition ratios in the solid (red, red scale) and melt (brown, red scale) of the Fe-C system. The blue square represents activity C, corresponding to the composition of $X(CH_4)$ = 0.1 in experiment 2177; the horizontal dotted line represents the composition of Fe-C in experiment 2177**.**

Figure 4 shows the calculated curve of dependence of the composition of a binary fluid ($X(CH_4)$ + $X(H_2)$ = 1) on the activity of carbon (relative to graphite) in the metallic phase at fixed values T=1523 K and P = 100 MPa (blue curve, left ordinate axis in Figure 4). Fig. 3. Image in backscattered electrons (BSE) of a cross-section of a metal ball from experiment 2177. The points are the numbers of the analyses in Table 3.

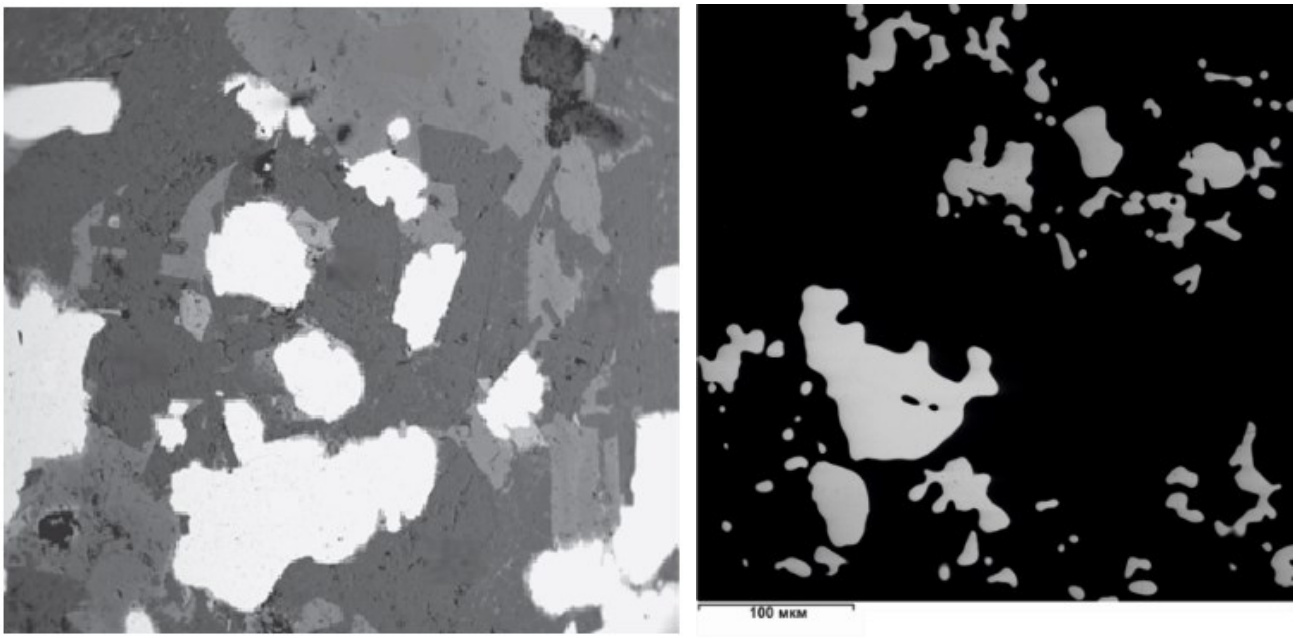

Fig. 5. Microcrusted iron in the rock–forming minerals of dolerites (white color is a metallic alloy of iron, gray and black color is a rock). Aikhal intrusive: mod. Ai-1. (Tomshin et al., 2023)

Fig. 6. Image in backscattered electrons (BSE) of a quenching sample after experiments on the interaction of a basalt melt with a hydrogen-methane fluid (experiment 2179): light – metallic iron alloy, black – basalt glass.

Conclusion

1. Geologists have established that trap intrusions with the appearance of native iron are widespread on the Siberian platform. According to Yakut geologists, the formation of native iron is based on the fluid-magmatic interaction of magma matter with the reducing components of the fluid, mainly of methane-hydrogen composition (Oleinikov et al., 1985; Tomshin et al., 2023; et al.).

2. It has been established that carbon, which is formed in experiments due to pyrolysis of CH_4, is dissolved in the metallic phase. Thus, the mechanism responsible for the presence of carbon in native iron in nature has been experimentally substantiated.

3. It has been experimentally established that the complex process of metal-silicate liquation in magmatic melts during their interaction with a methane-hydrogen fluid can be carried out at real magma temperatures in nature (≤ 1250 °C), significantly lower than the corresponding melting temperatures of iron. The entry of impurities of P, Ni, Co and, in particular, C can lower the melting point and can lead to the formation of true liquation structures.

The work was carried out within the framework of the research project No. FMUF-2022-0004 of Academician D.S. Korzhinsky Institute of Experimental Mineralogy of the Russian Academy of Sciences.

References:

Bird J.M., Goodrick C.A., Weathers M.S. (1981) Petrogenesis of Uiviaq iron, Disko Island, Greenland. J. Geophys. Res. B 86 (12), 11787-11806.

Oleynikov B.V., Okrugin A.V., Tomshin M.D. et al. (1985) Native metal formation in platform bases. Edited by V.V. Kovalsky. Yakutsk: YAF SB of the USSR Academy of Sciences, 124 p.

Ryabov V.V., Pavlov A.L., Lopatin G.G. (1985) Native iron of Siberian traps. Novosibirsk: Nauka SB RAS, 167 p.

Tomshin M.D., Kopylova A.G., Vasilyeva A.E. Native iron in Siberian traps. (2023) Petrology, volume 31, No. 2, p. 20-35

Rusak A.A.[1], Alferyeva Y.O.[2], Dushenko N.V.[1], Fedulov V.S.[1], Shchekina T.I.[2] Study of water solubility in acidic fluorine-containing glasses by IR and Raman spectroscopy. *UDC 552.08, 552.12*

[1]Vernadsky Institute of Geochemistry and analytical chemistry RAS (GEOKHI RAS), Russia, 119991, Moscow, st. Kosygina, 19, aleks7975@yandex.ru, [2]Lomonosov Moscow State University, Department of Geology, Russia, 119991, Moscow, st. Leninskiye gory, 1, t-shchekina@mail.ru,

Abstract. The work is aimed at determining the solubility of water in fluorine-containing quartz-normative aluminosilicate melts. Experiments were carried out at 800°C and 1 kbar with different initial contents of water (3, 5, 7 wt. %) and fluorine (0, 4, 8 wt. %) in the system and

a constant Si/Al/Na/Li ratio close to the composition of deeply differentiated topaz-bearing granites. The experimental products are represented by transparent porous aluminosilicate glass. IR and Raman spectroscopy were used to estimate the water content in the aluminosilicate glass. According to the IR spectroscopy data, three main regions are distinguished: the region of 1400-1800 cm^{-1}, which corresponds to vibrations of bonds of surface-adsorbed molecular H_2O on the surface of aluminosilicate glass; the region of 3450-3800 cm^{-1}, responsible for surface-absorbed water, with the addition of asymmetric vibrations of OH-groups and the region of 3200-3450 cm^{-1}, in which 3 characteristic absorption ranges were found (3212-3275 cm^{-1}, 3338-3383 cm^{-1}, 3411-3438 cm^{-1}). It is assumed that the manifestation of these 3 ranges is due to the fact that the hydroxyl group was chemisorbed into the structure of aluminosilicate glass, or that it was able to occupy an existing vacancy in the crystal structure of the glass. According to the Raman spectroscopy data, almost all the spectra of the samples we obtained are in the range of Raman shift values from 600 to 4000 cm^{-1}. Vibrations of the bond of silicon (or aluminum) with oxygen are reflected in the spectrum in the range of 700-1280 cm^{-1}. The oscillations of the O-H and H_2O bonds are reflected in the range of 2800-3720 cm^{-1}. In the absence of fluorine in the system, the amount of water dissolved in the melt does not exceed 2,4 wt. %. With an initial fluorine content of 7-8 wt. %, the amount of dissolved water increases to 6-7 wt. %. In the conducted series of experiments, the appearance of a fluid phase was not recorded. A further increase in the initial water content in the system can lead to an increase in the concentration of water in the melt.

***Keywords**: water solubility, fluorine-containing aluminosilicate glasses, IR spectroscopy, Raman spectroscopy, molecular water, hydroxyl group*

The aim of the work is to estimate the possible water content in deeply differentiated granite melts. In this regard, the objective of this work is to determine the solubility of water in model acidic fluorine-containing glasses using IR and Raman spectroscopy.

Nine experiments were carried out in platinum ampoules on a high gas pressure setup (UVGD-10000) at the IEM RAS at 800°C and 1 kbar with different initial contents of water (3, 5, 7 wt. %) and fluorine (0, 4, 8 wt. %) in the system and a constant Si/Al/Na/Li ratio close to the composition of topaz-bearing granites. The initial compositions of the experiments are presented in Table 1. The duration of the experiments ranged from 3 to 7 days. The accuracy of temperature maintenance was ±5°C, pressure ±0,05 kbar.

The chemical composition of the experimental products was determined in the laboratory of local methods for studying substances of the Department of Petrology and Volcanology of the Geological Faculty of Moscow State University using a Jeol JSM-6480LV scanning electron microscope with an Inca Energy-350 energy-dispersive spectrometer. Electron images were obtained in the reflected electron mode at an accelerating voltage of 20 kV. Local quantitative energy-dispersive analysis of phases was performed at an accelerating voltage of 20 kV and an electron probe current of 0,7 nA. The dispersion characterizing the detection threshold is 0,05 wt. % for F and 0,02 wt. % for Na, Al, Si.

Table 1. Initial compositions of the experiments.

Experience number	H_2O, wt. %	Composition of dry sample (wt. %)					
		Si	Al	Na	Li	F	O
RsF_0Wt_3	3	34,77	9,01	6,18	0,06	0,00	49,97
RsF_0Wt_5	5	34,77	9,01	6,18	0,06	0,00	49,97
RsF_0Wt_7	7	34,77	9,01	6,18	0,06	0,00	49,97
RsF_4Wt_3	3	33,97	8,80	6,04	0,06	4,00	47,13
RsF_4Wt_5	5	33,97	8,80	6,04	0,06	4,00	47,13
RsF_4Wt_7	7	33,97	8,80	6,04	0,06	4,00	47,13
RsF_8Wt_3	3	33,16	8,59	5,90	0,06	8,00	44,29
RsF_8Wt_5	5	33,16	8,59	5,90	0,06	8,00	44,29
RsF_8Wt_7	7	33,16	8,59	5,90	0,06	8,00	44,29

The amount of water in the glasses was determined using Raman spectrometry. The data on Raman scattering were obtained in the range from 600 to 4000 cm^{-1}. The stretching vibrations of the bond of silicon (or aluminum) with oxygen are reflected in the spectrum in the range of 680-1280 cm^{-1}. The vibrations of the O-H and H_2O bonds are reflected in the range of 2800-3720 cm^{-1}. For the standards of quartz-normative fluorine-containing glasses with known water content, a graph of the correspondence between the amount of water and the ratio of the areas of the peaks 2800 - 3720 cm^{-1} and 680 - 1280 cm^{-1} was constructed. A quantitative estimate of the water content in the studied glass samples is obtained by comparing the calculated ratios of the areas of these peaks with the values in

standard glasses (Chabiron, 2004, etc.).

The experimental products are represented by porous transparent aluminosilicate glass (Fig. 1). In some glasses with a fluorine content of more than 4 wt. %, quartz crystals (up to 2 vol. %) were found (Fig. 2), which have an isometric shape with subhedral outlines. Quartz often forms clusters confined to the edge of the sample. The chemical composition of aluminosilicate glasses is presented in Table 2.

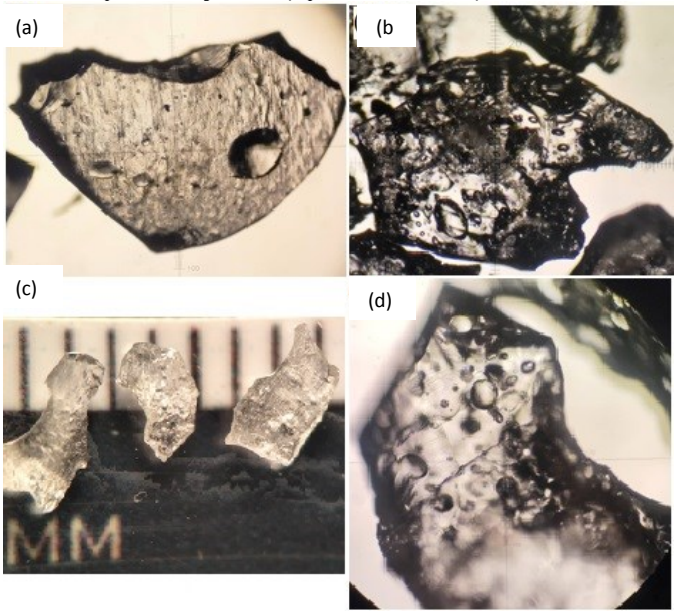

Fig. 1. External appearance of some samples of aluminosilicate glasses: a) RsF_8Wt_7; b) RsF_8Wt_3; c-d) RsF_4Wt_7. The images were obtained using a Mikromed MC-2 Zoom optical binocular (Fig. 1c) and an Olympus BX51 optical microscope (Fig. 1a, b, d).

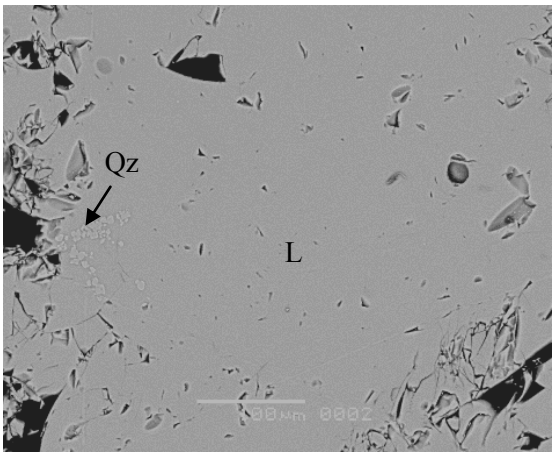

Fig. 2. A section of homogeneous aluminosilicate glass (L) and a cluster of quartz crystals (Qz) on the left side of sample RsF_4Wt_7. BSE image.

Table 2. Composition of aluminosilicate glasses recalculated for oxygen and water (wt. %).

Experience number	Phase composition	SiO_2	Al_2O_3	Na_2O	F	O=2F	Sum	H_20
RsF_0Wt_3	L	77,20	12,30	5,81	0,00	-	97,38	2,02
RsF_0Wt_5	L	76,26	12,93	5,98	0,00	-	97,56	2,38
RsF_0Wt_7	L	77,96	12,09	5,73	0,00	-	97,51	1,69
RsF_4Wt_3	L+Qz	71,77	13,30	7,04	3,97	1,67	96,66	2,19
RsF_4Wt_5	L+Qz?	67,79	13,34	6,56	3,41	1,44	95,94	6,03
RsF_4Wt_7	L+Qz	69,04	13,77	7,31	4,11	1,73	97,72	5,13
RsF_8Wt_3	L+Qz	65,21	15,49	8,42	8,43	3,55	97,71	3,61
RsF_8Wt_5	L+Qz	63,97	13,73	7,44	7,45	3,13	96,88	7,23
RsF_8Wt_7	L+Qz?	65,48	13,60	7,17	6,97	2,94	96,22	5,67

Note. The name of the experiment includes data on the fluorine and water content, for example, RsF_0Wt_3, where F_0 is the fluorine content of 0 wt. %, and Wt_3 is the water content of 3 wt. %, etc.

It is evident from Table 2 that the addition of fluorine to the haplogranite system leads to a shift in the melt composition to the low-siliceous region. This is due to the appearance of quartz. The expansion of the crystallization field of this mineral occurs as a result of the shift in the eutectic composition of the system as the fluorine content increases.

The measured amount of water in the glasses depends on the initial fluorine content. In the absence of fluorine in the system, the amount of water dissolved in the melt does not exceed 2,4 wt. %. With an initial fluorine content of 8 wt. %, the amount of dissolved water increases to 6-7 wt. %. Since no fluid phase was detected in the series of experiments, a further increase in the initial water content in the system may lead to an increase in the water concentration in the silicate melt. The results

of the study of the IR spectra of fluorine-containing silicate glasses are presented in the works (Kumar et al., 1961; Weisfeld, Rabinovich, 1962; Kogarko, Krigman, 1981, etc.). In the work (Kogarko, Krigman, 1981), it is shown that it is practically impossible to explicitly identify the ≡Si—F bonds in the IR spectra. However, in the work (Kumar et al., 1961) it was stated that for the glass Na-17 + F a characteristic signal (764 cm^{-1}) was detected, caused by the formation of the bond ≡Si—F. In the work (Weissfeld, Rabinovich, 1962) for the series of glasses M-40 + F a similar result was obtained (700÷800 cm^{-1}), confirming the formation of groups [SiO_4-αFα]. In our case, in the samples RsF_8Wt_3 and RsF_8Wt_7 a stable signal of low intensity was detected in the region of 707-730 cm^{-1}.

Three main regions are distinguished: the region of 1400-1800 cm^{-1}, which corresponds to the vibrations of the bonds of surface-adsorbed molecular H_2O on the surface of aluminosilicate glass; the region of 3450-3800 cm^{-1}, responsible for surface-absorbed water, with the addition of asymmetric vibrations of OH-groups and the region of 3200-3450 cm^{-1}, in which 3 characteristic absorption ranges were found (3212-3275 cm^{-1}, 3338-3383 cm^{-1}, 3411-3438 cm^{-1}), which imply that the hydroxyl group was either chemisorbed into the glass structure, or it was able to occupy an existing vacancy in the crystal structure of the glass (Fig. 3).

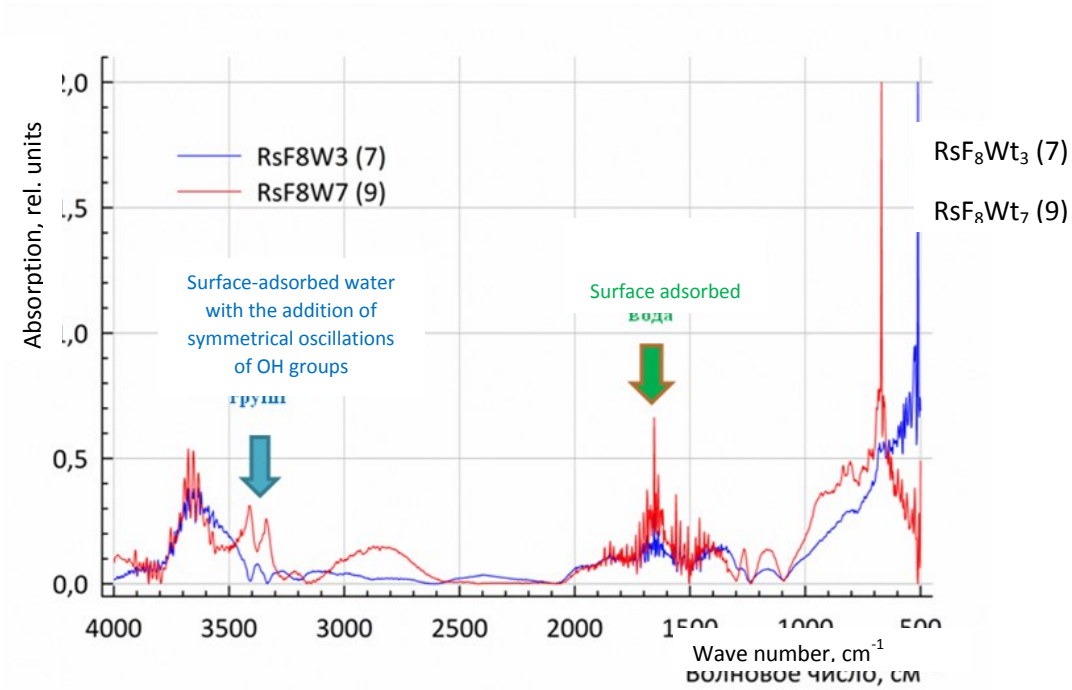

Fig. 3. IR spectra for RsF_8Wt_3 and RsF_8Wt_7 samples with highlighted areas of surface-absorbed water with the addition of asymmetric vibrations of OH-groups and surface-adsorbed molecular water.

Conclusions. According to Raman spectroscopy data, it is shown that in the absence of fluorine in the system, the amount of water dissolved in the melt does not exceed 2,4 wt. %. With an initial fluorine content of 8 wt. %, the amount of dissolved water increases to 6-7 wt. %. Probably, such a water content is not the saturation limit and a further increase in its amount in the system will lead to an increase in the concentration of water in the melt. According to IR spectroscopy data, areas of surface-absorbed water were detected, in which three characteristic absorption ranges were found (3212-3275 cm^{-1}, 3338-3383 cm^{-1}, 3411-3438 cm^{-1}), which imply that the hydroxyl group was either chemisorbed into the glass structure or was able to occupy an existing vacancy in the crystal structure of the glass. Thus, it is shown that water is built into the glass structure in the form of OH-groups.

Funding sources. The work was carried out within the framework of the state assignment of the GEOKHI RAS and on the state budget theme "Regimes of petrogenesis of the Earth's internal geospheres" of the Geological Faculty of the Lomonosov Moscow State University.

References

Weisfeld N. M., Rabinovich E. M. Electron microscopic study of fluoride and phosphate opal glasses // Zh. Phys. 1962. Vol. 35. № 11. PP. 2393–2399. [in Russian]

Kogarko L. N., Krigman L. D. Fluorine in silicate melts and magmas. Moscow: Nauka, 1981. 127 p. [in Russian]

Chabiron A., Pironon J., Massare D. Characterization of water in synthetic rhyolitic glasses and natural melt inclusions by Raman spectroscopy //Contributions to Mineralogy and Petrology. 2004. V. 146. P. 485–492.
Kumar D., Ward R. G., Williams D. J. Effect of fluorides on silicates and phosphates // Discuss. Farad. Soc. 1961. N 32. P. 147–154.

Shchekina T.I.[1], Zinovieva N.G.[1], Alferyeva Ya.O.[1] Kotelnikov A.R.[2], Rusak A.A.[3] Behavior of the main rock-forming elements, tungsten and molybdenum during the interaction of granite melt with dolomite at 700 °C and P_{H_2O}= 1 kbar in the presence of fluorine. *UDC 552.113*

[1] Geological Faculty, Lomonosov Moscow State University, Moscow [2]Institute of Experimental Mineralogy named after D.S. Korzhinsky Institute of Geochemistry and Analytical Chemistry of the Russian Academy of Sciences, Chernogolovka [3]Vernadsky Institute of Geochemistry and Analytical Chemistry of the Russian Academy of Sciences, Moscow t-shchekina@mail.ru, nzinov@mail.ru, YanaAlf@bk.ru kotelnik1950@yandex.ru aleks7975@yandex.ru

Abstract. The experiments conducted simulate the formation of magnesian skarns. Their main feature is the formation of reaction metasomatic formations during the direct interaction of granite F-containing melt and carbonate, represented by dolomite. Skarn zoning of the magmatic stage of interaction of aluminosilicate melt and carbonate rock was experimentally simulated. The behavior of the main rock-forming (Si, Al, Ca, Mg, Na, K), rare elements (Mo and W) and fluorine in all zones of the column was studied and their mobility under experimental conditions was estimated. The similarity of the metasomatic column structure and mineral composition of the zones obtained in the experiment with those formed in magnesian skarns is shown.

***Keywords**: skarn zoning, magnesian endoskarn, exoskarn, molybdoscheelite, magmatic stage of interaction, aluminosilicate melt, carbonate rock, dolomite*

Experiments were carried out on the interaction of F-containing granite melt with dolomite, simulating the formation of magnesian skarns of the magmatic stage with the participation of rare elements.

Experimental and phase analysis technique. The experiments were carried out at a temperature of 700°C and 1 kbar in the presence of water in an amount of 10 wt. % on the high gas pressure setup at the IEM RAS. The error in temperature measurement is ±5°C and pressure ±10 bar. Oxygen fugacity in the experiments corresponded to the NNO buffer. The quenching rate was 150–200 deg/min. Granite glass containing 4 wt. % F was placed at the bottom of 5 mm diameter Pt ampoules. Dolomite powder consisting of thoroughly mixed and compacted CaCO3 and MgCO3 reagents was placed above it, and 10 wt. % distilled water was poured in. Then the ampoule was welded. After the experiment had been running for 7 days at 700°C and 1 kbar, the experiment was quenched. When the ampoule was opened, a column of substance with clearly defined contact between two media was found: hardened gray glass and light fine-grained carbonate-silicate material. The experimental products were filled with epoxy resin and polished. The contents of rock-forming elements, fluorine and oxygen were determined using a Jeol JSM-IT500 scanning electron microscope (Jeol, Japan) with an Oxford X-MaxN energy-dispersive spectrometer (Oxford Instrument Ltd., UK) and a Superprobe JXA-8230 electron probe microanalyzer (Jeol, Japan) in the laboratory of local methods for studying matter at the Department of Petrology and Volcanology of the Geological Faculty of Moscow State University. After the experiments, 9 zones were identified in the sample, five of them in the endo- and four zones in the exocontact area.

The thickness of the obtained column (Fig. 1 a-g) is ~ 6 mm: 2.5 mm of which are endoskarn zones, including hardened glass, and 3.5 mm are exoskarn zones. The contacts between the endoskarn zones are very clear (Fig. 1a). They are all monomineral. We attribute granite glass to the first zone of the column, and the rim of alkali feldspar $(Na_{0.27}K_{0.71})Ca_{0.01}Al_{1.03}Si_{2.92}$ with glass, which formed at the melt-carbonate boundary, to the second zone. A crack 20 to 200 μm wide formed between the granite melt (zones 1, 2) and the carbonate during quenching. It is filled with detrital material of minerals from the endodocontact zones (3-5). These zones are composed of newly formed minerals, respectively, mullite $Al_{3.62}Si_{1.24}O_8$ (zone 3), basic plagioclase (zone 4) $(Na_{0.37}K_{0.03}Ca_{0.60})(Al_{1.59}Si_{2.4})O_8$, and fluorphlogopite $K_{0.91}Na_{0.17}Ca_{0.02}Fe_{0.14}Mg_{3.07}(Al_{1.24}Si_{3.19})(OH,F)_2O_{10}$ (zone 5). No reaction relationships are observed between the endocontact zones. The average composition of the quenched granite glass (Table 2) changes insignificantly with respect to the rock-forming components as it approaches the contact with the carbonate substance. The most important change in the initial composition of the granite melt is a significant decrease in the fluorine content to 0.83% after the experiment compared to the 4 wt.% introduced into the glass. It can be concluded that fluorine is intensively removed from the granite melt during interaction with the carbonate material. Fluorine is part of the minerals of the interaction column that formed: in the endoskarn part, it is part of fluorophlogopite, and in the exoskarn part, it is part of humite.

Table 1 shows the compositions of glasses (quenched melts) - pure glass without crystals and

glass with quartz and feldspar crystallizing from it.

In the exocontact zone, significant changes in the mineral composition of the carbonate material occur. They reflect the process of reaction interaction of dolomite with fluids coming from the granite melt. Thus, in the first exocontact zone along the section (zone 6 in Table 1, Fig. 1a), dolomite completely disappears, being replaced by calcite $Ca_{0.99}Mg_{0.01}CO_3$, along which wollastonite in turn begins to develop (Fig. 2). In this case, Mg is part of the newly formed clinopyroxene and a small amount of opthopyroxene. In the next zone 7 (Fig. 1 b) the process of replacement of calcite by wollastonite and crystallization of a larger amount of clinopyroxene continues. Its composition corresponds to diopside $Ca_{1.01}Mg_{1.03}Si_{1.9}O_6$. Humite is formed inside the pyroxene grains (Fig. 1c), the composition of which closely corresponds to the formula $3Mg_2[SiO_4]xMgF_2$. Orthopyroxene is also present in this zone. Zone 7 has a maximum length in the column of about 800 μm.

Table 1. Column diagram by interaction zones

	Mineral composition and thickness of endoskarn zones (in μm)				
Zone	1	2	3	4	5
L, μm	2400	20	30	20	5
Phases	L	L+Fsp	Mul	Pl	F-Phl
	Mineral composition and thickness of endoskarn zones (in μm)				
Zone	6	7	8	9a	9b
L, μm	600	800	1100	400	600
Phases	Cal+Wol+Cpx+Opx	Cpx+Wol+Hu+Opx	Cpx+Hu+Wol+Cal	Cal+Hu	Dol+Hu

Table 2. Average composition of aluminosilicate glass after the experiment

Glass 1 pure without crystallizing phases											
Components	SiO_2	Al_2O_3	FeO	MgO	CaO	Na_2O	K_2O	WO_3	MoO_3	F	Sum
Xcp	73,02	12,38	0,34	0,12	0,18	1,76	4,20	0,43	0,13	0,73	92,97
S	0,12	0,09	0,11	0,03	0,02	0,61	0,53	0,07	0,01	0,02	1,24
Glass 2 with capture of crystallizing phases (area analysis)											
Xcp	73,27	11,70	0,45	0,13	0,16	1,80	4,12	0,86	0,19	0,80	93,14
S	3,23	1,70	0,22	0,05	0,06	0,60	0,57	0,45	0,09	0,23	0,91

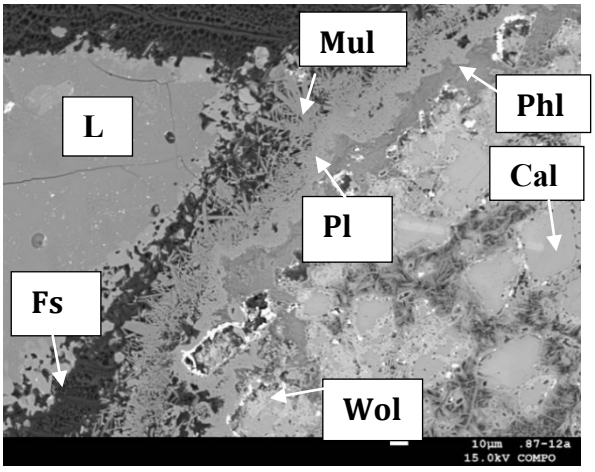

Fig. 1a. Endocontact zones - 1-5; exocontact zone 6 - Cal (calcite) + Wol (wollastonite) + Cpx and Opx (clino- and orthopyroxene), Mul (mullite)

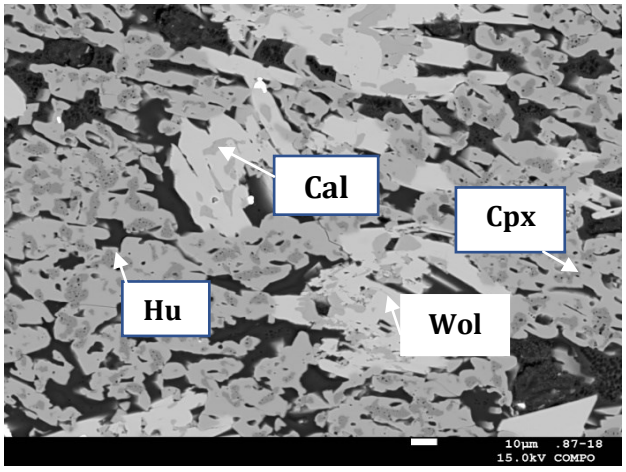

Fig. 1b. Exocontact zone 7: Cpx (clino-) and Opx (orthopyroxene) + Cal (calcite) + Wol (wollastonite) + Hu (humite)

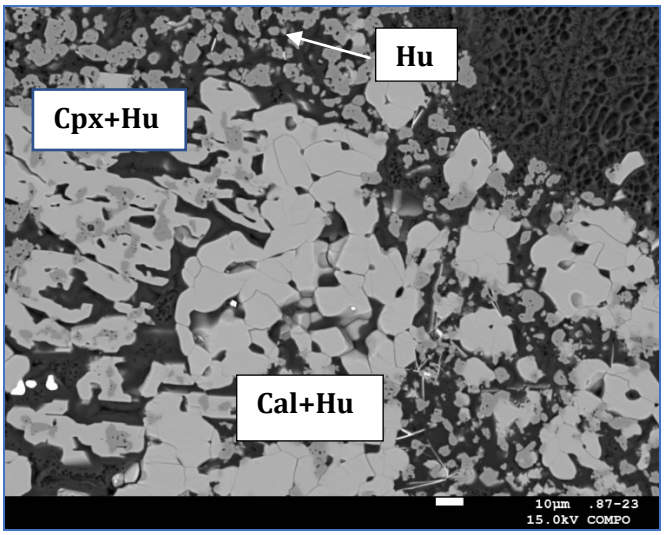

Fig. 1c. Contact of zones 8 (Cpx + Hu) and 9a (Cal+Hu) of the exoskarn

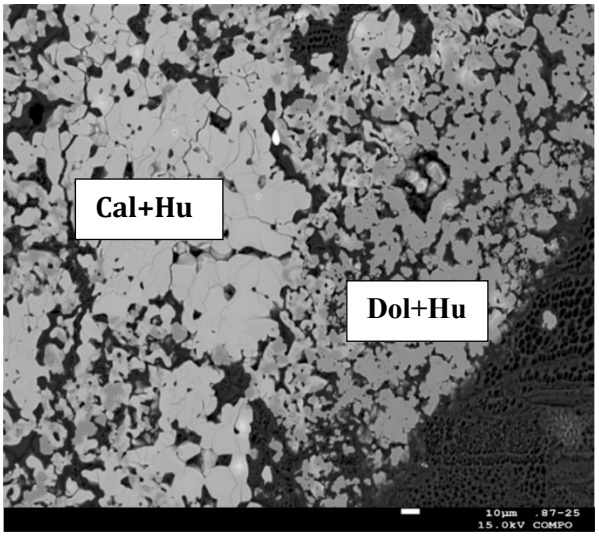

Fig. 1d. Contact of zones 9a (Cal(calcite)+Hu (humite) and 9b (Dol+Hu)

When moving to zone 8, clinopyroxene and humite begin to predominate in the mineral composition, sometimes forming clusters of small crystals of 5-10 µm (Fig. 1c). The proportion of calcite in the eighth zone is no more than 20-30%. The last zone of column 9b is composed mainly of dolomite, but the transition to dolomite occurs through a zone consisting of calcite and humite (9a), with a thickness of about 200 µm. The presence of humite indicates the diffusion of Si up to the last endoskarn zone. It should be noted that the fluorine content in humite along the column section is 2-3 wt. % in the first zones, increases to 5 wt. % in the middle and up to 8 wt. % in the last exoskarn zone, which indicates an increasing degree of fluorine diffusion from the granite melt into carbonate part of the column to its end. The ratio of Ca to Mg in carbonates also changes along the interaction column. If in the exoskarn zone closest to the granite melt, the carbonate is represented by almost pure calcite, then as it moves away from the contact, it an increase in the magnesium content is observed up to the last zone 9b, composed of dolomite with the composition $Mg_{0.48}Ca_{0.52}CO_3$. The structure of the column and its mineral composition, studied in experimental samples, are very similar to those observed in nature in magnesian skarns (Khitarov et al., 1962; Shabynin, 1973; Zaraysky, 1989; Pertsev, 1998; Alferyeva et al., 2024).

Of particular interest is the behavior of W and Mo during the contact interaction of granite melt and carbonate. 0.23 wt. % W and 0.2 wt. % Mo were introduced into the glass in the form of oxides. Judging by the photographs, it is evident that among the silicate and carbonate phases of the interaction column, scheelite or molybdoscheelite grains 2-4 µm in size are found in all zones. The largest amount of scheelite with the highest ratio W/(W+Mo) = 0.88-0.92 was found in the endo-skarn (phlogopite) fifth zone of the column. Small grains usually form a rim at the boundaries of pores in the sample. In the exoskarn zones of the column, molybdoscheelite most often crystallizes at the boundaries of carbonate and silicate phases (Fig. 1): in the first calcite-wollastonite zone, it was found at the contact of large calcite grains and aggregates of pyroxene grains (Fig. 1a), forming chains of small white (in BSE) grains along the boundaries of minerals. In the endo-contact zone, molybdoscheelite contains the largest amount of tungsten. With increasing distance from the contact, the content of the powellite component in the molybdoscheelite increases. In the very last 9th zone of the exoskarn, only single grains were found, represented by powellite with a ratio of W/(W+Mo) = 0.07.

Conclusions

1. A column of interaction of F-containing granite melt with dolomite, similar to natural objects, was obtained, and the behavioral features of chemical elements in it were revealed.

2. Silicon actively migrates along the column up to its end, entering into all newly formed silicates (wollastonite, pyroxene, humite), while its content gradually decreases.

3. The aluminum content forms a maximum at the contact of endo- and exocontact zones and then sharply decreases in the exoskarn area.

4. Magnesium diffuses from dolomite into the endoskarn zone, entering into F-phlogopite, and in the exoskarn zone it is recorded in humite, clino- and orthopyroxene. Dolomite is preserved only in the last zone of the exoskarn in paragenesis with humite.

5. The calcium concentration increases sharply in the contact zone of the granite melt and dolomite: a zone of basic plagioclase is formed in the endocontact area, and calcite, wollastonite and clinopyroxene in the exoskarn zone.

6. Fluorine almost completely leaves the granite

melt and is fixed throughout the column, entering into the composition of fluorphlogopite in the endoskarn zone and in the composition of humite in all exoskarn zones.

7. W and Mo diffuse from the granite melt and precipitate as molybdoscheelite in the endo- and exocontact zones throughout the column, especially effectively in the endo- and first exoskarn zones. Tungsten concentrations in molybdoscheelite are higher within the endocontact zones, and molybdenum contents are higher in the last exocontact zones, which indicates greater mobility of Mo in the metasomatic process.

The study was carried out within the framework of the state assignment of Lomonosov Moscow State University, IEM RAS and GEOKHI RAS. We thank the staff of the shared use center "Electron probe microanalysis of mineral matter" (Geological Faculty of Moscow State University, Department of Petrology and Volcanology) for assistance in studies on a JSM-IT500 scanning electron microscope (Jeol, Japan) with an Oxford X-MaxN energy-dispersive spectrometer (Oxford Instrument Ltd., UK) and a JEOL JXA-8230 electron probe microanalyzer, purchased using funds from the "Moscow University De LIST OF

References

1. Zarayskiy G.P. Zoning and conditions of formation of metasomatic rocks. Moscow: Nauka. 1989. 341 p.
2. Pertsev N.N. Acid-base interaction of silicate magmas with carbonate rocks. DAN. 1998. Vol. 362. No. 1. Pp. 102-105.
3. Khitarov N.I., Lebedev E.B. Lebedeva R.V. Experimental data on the characteristics of the formation of skarns containing wollastonite. In the book: Experimental studies in the field of deep processes. Moscow: Publ. USSR Academy of Sciences, 1962, pp. 43-54.
4. Shabynin L.I. Formation of magnesian skarns. Moscow: Nauka. 1973. 214 p.
5. Alferyeva Ya.O. Gramenitskiy E.N., Novikova A.S. Experimental Modeling of Interaction between Fluorine-Containing Granite Melt and Calcite Marble. Petrology, 2024, Vol. 32, N 2, PP. 236–248.velopment Program"

Suk N.I., Kotelnikov A.R. Experimental study of sphalerite solubility in aluminosilicate melts at T=900 °C and P=2 kbar. *UDC 550.89:549.08*

IEM RAS, Chernogolovka, Moscow region
(sukni@iem.ac.ru; kotelnik1950@yandex.ru)

Abstract. The solubility of sphalerite (ZnS) in aluminosilicate melts of different alkalinity was studied experimentally at T=900°C and P=2 kbar in dry conditions and in the presence of 10 wt. % H_2O. It was found that the solubility of sphalerite depends on the composition of the aluminosilicate melt, increasing with increasing its agpaiticity ((Na+K)/Al). At the initial agpaiticity of the glass of ~1.5, a sulfide melt is formed in dry systems, while the alkalinity and Zn content in the glass increase. At the initial agpaiticity of the glass of ~2, the formation of zinc sulfide crystals is observed, differing in composition from the initial sphalerite. In water-containing systems, partial oxidation of sulfide sulfur to sulfate sulfur occurs with the formation of drop-shaped precipitates of an alkaline sulfate melt.

***Keywords**: sphalerite, aluminosilicate melt, experiment*

The solubility of sphalerite (ZnS) in aluminosilicate melts of varying alkalinity was studied experimentally at T=900°C and P=2 kbar in dry conditions and in the presence of 10 wt. % H_2O. The experiments were carried out on a high-gas-pressure vessel. The duration of the experiments was 10 days. The starting material was fused granite glass of varying agpaiticity (1–2.5), as well as natural sphalerite with the composition corresponding to the formula $Zn_{0.92}Fe_{0.08}S_{0.99}$. The composition of the samples after the experiments was determined by electron probe X-ray spectral analysis.

As a result of the experiments in dry systems, a glass column with sphalerite crystals was obtained (Fig. 1).

It was found that the solubility of sphalerite depends on the composition of the aluminosilicate melt, increasing with increasing agpaiticity ((Na+K)/Al) (Fig. 2). The compositions of the experimental glasses obtained are presented in Table 1.

With the initial agpaiticity of the glass of ~1.5, in dry systems a sulfide melt is formed (Fig. 3) of the following composition (wt.%): Zn – 48.06, Fe – 18.38, S – 33.56. In this case, the alkalinity and Zn content increase in the glass (Table 1, Z-2*). The formation of small crystals corresponding to the average composition of $Zn_{0.87}Fe_{0.14}S_{0.99}$ is also observed. With the initial agpaiticity of the glass of ~2, the formation of zinc sulfide crystals is observed, differing in composition from the initial sphalerite, their composition corresponds to the formula $Zn_{0.87}Fe_{0.08}Mn_{0.06}S_{0.99}$.

In water-containing systems, partial oxidation of sulfide sulfur to sulfate sulfur occurs with the formation of drop-shaped precipitates of alkaline sulfate melt (Fig. 4). Crystals of alkali sulfates are observed within the sulfate melt. Large crystals of alkali zinc silicates also form in the glass (Fig. 4, Table 2), the number and size of which increase with the growth of the initial agpaiticity of the melts. In this case, the agpaiticity coefficient (Kagp) of the glass decreases on average to 1.1 regardless of the initial agpaiticity, and the zinc oxide content increases to ~2.7-5.3 wt.%, which is higher than in dry systems with similar alkalinity.

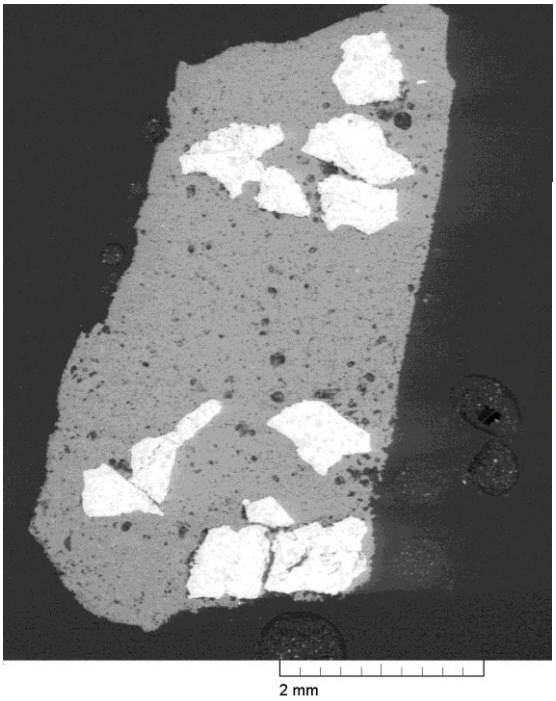

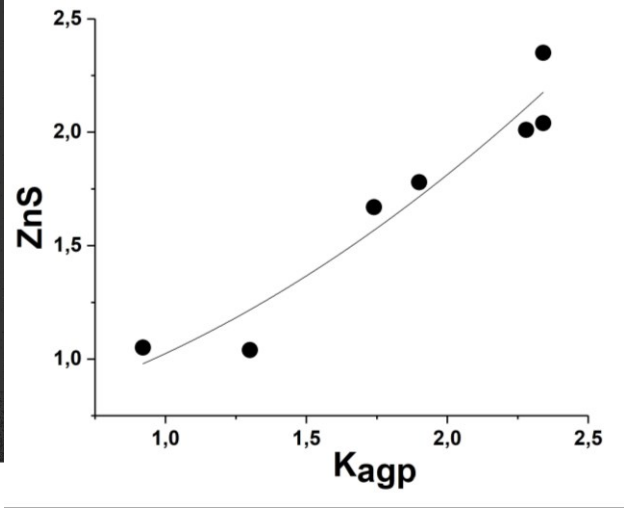

Fig. 1. Sphalerite crystals in aluminosilicate glass obtained in an experiment at T=900°C, P=2 kbar in a dry system (sample Z-1).
Fig. 2. Dependence of sphalerite solubility on the composition of aluminosilicate melt (wt.%) in dry systems at T=900°C, P=2 kbar.

Table 1. Glass compositions in experiments on sphalerite solubility in dry systems at T=900°C, P=2 kbar

Oxides	Z-1 n=13	Z-2* n=16	Z-2 n=9	Z-3 n=19	Z-3 n=13	Z-3 n=6
SiO_2	72.60	59.03	71.72	63.21	65.09	59.13
Al_2O_3	15.39	9.84	13.53	13.34	13.76	12.45
MgO	-	-	-	0.33	0.11	0.80
FeO	0.22	11.70	0.34	0.97	0.47	2.05
MnO	-	0.25	-	1.50	0.81	2.97
CaO	0.17	0.26	0.16	0.25	0.21	0.35
Na_2O	4.85	10.33	5.93	9.57	8.38	12.15
K_2O	5.72	5.53	7.27	8.83	9.34	7.71
ZnO	1.05	2.35	1.04	1.78	1.67	2.01
SO_3	-	0.72	-	0.23	0.16	0.38
Sum	100	100	100	100	100	100
Kagp	0.92	2.34	1.30	1.90	1.74	2.28

Note: * Glass composition near sulfide melt precipitates.

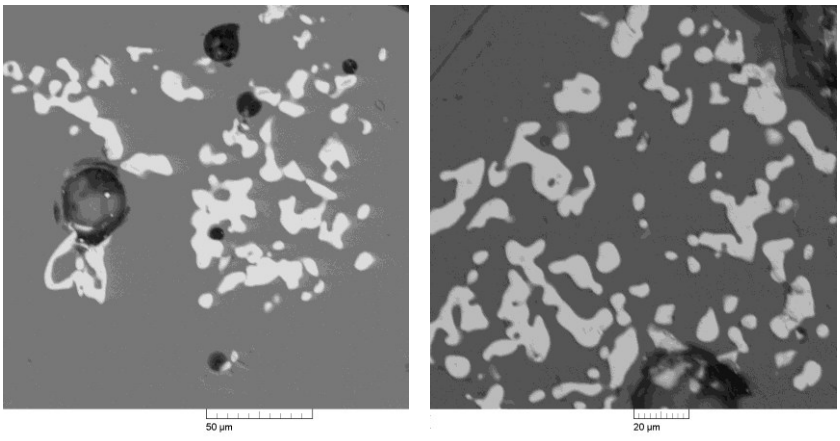

Fig. 3. Segregation of sulfide melt in a dry system at T= 900°C and P=2 kbar (sample Z-2).

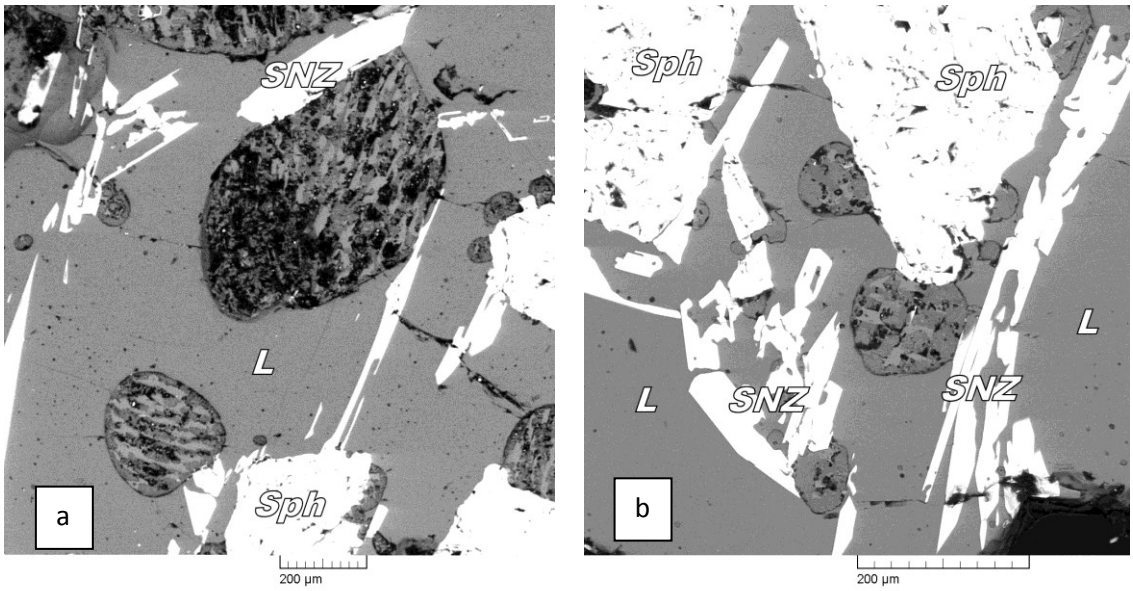

Fig. 4. Alkaline sulfate melt separations in an aluminosilicate matrix and newly formed crystals of alkali zinc silicates in a water-containing system at T= 900°C and P=2 kbar. a, b – sample Z-6. Sph – sphalerite, SNZ – alkali zinc silicate, L – mel**t.**

Table 2. Compositions of newly formed crystals of alkali zinc silicates in experiments on sphalerite solubility at T=900°C, P=2 kbar

Oxides	Water-containing systems		
	Z-4	Z-5	Z-6
	n=1	n=6	n=4
SiO_2	25.97	24.28	23.43
FeO	1.61	1.65	1.82
MnO	0.36	0.31	0.52
Na_2O	10.69	8.00	8.95
ZnO	61.68	65.77	65.29
Sum	100	100	100

The work was supported by the FMUF-2022-0004 program of the IEM RAS.